OPEN ACCESS
Fractals, Vol. 34, No. 6 (2026) 2640038 (24 pages)

DOI: 10.1142/S0218348X26400384

World Scientific
www.worldscientific.com

ADVANCED MATHEMATICAL ANALYSIS OF EBOLA VIRUS TRANSMISSION THROUGH FRACTAL FRACTIONAL-ORDER MODELS

ATEEQ UR REHMAN IRSHAD
Department of Mathematics and Sciences
Prince Sultan University, Riyadh 11586, Saudi Arabia
airshad@psu.edu.sa

NADEEM KHAN
School of Mathematics and Statistics
Central South University, Changsha 410083
Hunan, P. R. China
nadeemuom3@gmail.com

MUKHTIAR KHAN* and FARHAD HUSSAIN†
Department of Mathematics, University of Malakand
Chakdara Dir (L), 18000 Khyber Pakhtunkhwa, Pakistan
**mkhanuom2011@gmail.com*
†*farhadhussain447@gmail.com*

KAMAL SHAH
Department of Mathematics and Sciences
Prince Sultan University, Riyadh 11586, Saudi Arabia
Department of Mathematics, University of Malakand
Chakdara Dir (L), 18000 Khyber Pakhtunkhwa, Pakistan
kshah@psu.edu.sa

‡Corresponding author.

BAHAAELDIN ABDALLA
Department of Mathematics and Sciences
Prince Sultan University, Riyadh 11586, Saudi Arabia
babdallah@psu.edu.sa

KHURSHEED J. ANSAR
Department of Mathematics, College of Science
King Khalid University, 61413 Abha, Saudi Arabia
ansari.jkhursheed@gmail.com

THABET ABDELJAWAD ‡
Department of Mathematics and Sciences
Prince Sultan University, Riyadh 11586, Saudi Arabia
Department of Fundamental Sciences, Faculty of Engineering and Architecture
Istanbul Gelisim University, Avcilar 34310, Istanbul, Turkey
Department of Medical Research, China Medical University
Taichung 40402, Taiwan
tabdeljawad@psu.edu.sa

Received November 11, 2024
Accepted December 10, 2024
Published March 3, 2026

Abstract

This study presents an advanced mathematical framework for analyzing the intricate dynamics of Ebola virus transmission, utilizing a fractal–fractional order model to encapsulate the complex geometric characteristics of the underlying dynamical system. The existence and uniqueness of solutions are established through a rigorous fixed-point theorem approach, while Ulam–Hyers stability is meticulously investigated. Fundamental epidemiological insights are derived, including the establishment of non-negative solutions, computation of the basic reproduction number, sensitivity analysis, and identification of equilibrium points. To corroborate the theoretical results, numerical simulations are performed using the Adams–Bashforth approximation method, alongside the development of an interpolation-based numerical scheme to enhance computational efficiency. The findings are illustrated through comprehensive graphical representations, highlighting the robustness and applicability of the proposed model in elucidating and predicting the transmission dynamics of the Ebola virus.

Keywords: Ebola Virus Transmission; Stability Analysis; Existence and Uniqueness Theory; Numerical Simulation.

1. INTRODUCTION

Ebola virus disease (EVD) is a severe and often fatal illness caused by the Ebola virus, which is primarily associated with fruit bats as its natural reservoir.[1] The first recorded outbreak of Ebola occurred in Africa in 1976, with the virus being identified near the Ebola River in Zaire, from which it derives its name.[2] To date, researchers have identified six distinct species of the Ebola virus, four of which are known to cause diseases in humans. The virus poses a significant threat due to its high fatality rate and ability to cause severe illness and systemic dysfunction.[3,4] Ebola virus typically enters the human body through mucosal surfaces, skin abrasions, or other breaches in physical barriers. Once inside the body, it targets and disrupts multiple systems, including

the lymphatic system and epithelial cells, among others. The virus exhibits a latency period of approximately 3 to 21 days, during which it replicates extensively within host cells and triggers complex immune responses.[5] The progression of the disease is characterized by the onset of non-specific symptoms such as fever, vomiting, headache, and diarrhea, resulting from the viral destruction of host cells and tissues (Fig. 1). In advanced stages, the infection escalates to severe complications, including liver and kidney failure, which often lead to death. Prompt and effective medical intervention is therefore critical to mitigate organ damage and reduce mortality. Understanding the transmission dynamics and pathophysiology of Ebola virus is essential for developing robust models to predict outbreaks and inform public health strategies.[7–9]

EVD is a highly fatal illness requiring extreme caution in its prevention and treatment. Transmission occurs primarily through direct contact with the blood or bodily fluids of an infected individual. Thus, avoiding contact with infected persons, their belongings, and sterilizing medical equipment, clothing, and other materials are essential measures to limit the spread of the virus.[10] In addition, precautions such as avoiding sexual contact during the infection period are advised to mitigate transmission risks. Efforts to combat EVD have led to the development of various treatment strategies, including vaccines, and pharmacological therapies. Two licensed vaccines, administered as single-dose intramuscular injections, have demonstrated significant efficacy and safety in combating the virus. Notably, the VSV-EBOV vaccine, introduced in 2016, achieved a success rate of 95–100% in clinical trials.[11,12] These vaccines bolster immune system responses, particularly in vulnerable populations, offering an accessible and cost-effective alternative to high-dose treatments in resource-constrained settings.[13,14] Despite its rarity, Ebola remains a deadly disease with devastating consequences. Infections often result from direct contact with infected animals (e.g. monkeys, apes, and fruit bats) or contaminated medical equipment and bodily fluids from infected individuals or recently deceased patients.

Public health efforts in regions like Pakistan have included workshops and awareness programs to train healthcare professionals on effective management and prevention strategies for the disease. Mathematical modeling plays a crucial role in understanding and predicting the dynamics of EVD transmission, especially in settings with limited healthcare resources. Researchers have developed various compartmental models, such as the Susceptible-Infectious-Recovered (SIR) model, to analyze disease dynamics and evaluate control strategies.[15,16] Deterministic and stochastic models have been employed to study the spread and mitigation of the disease, with findings highlighting the importance of robust healthcare strategies.[17,18] Traditional models often rely on integer-order derivatives, which may oversimplify the biological memory and hereditary effects intrinsic to disease systems. In contrast, fractional calculus, which incorporates non-local and memory-dependent operators, offers a more comprehensive framework for modeling complex dynamics.

Fractional calculus has found widespread application across scientific fields due to its versatility, with commonly used operators including the Riemann–Liouville, Caputo, and Atangana–Baleanu derivatives.[19] These operators, characterized by kernels such as the power law, exponential decay law, and generalized Mittag-Leffler function, provide enhanced accuracy for modeling and simulation.[20–23] Fractal derivatives further extend the applicability of fractional calculus by capturing spatial complexity and self-similarity, making them particularly suitable for modeling real-world phenomena with intricate dynamics.[24–27]

Our study investigates the dynamics of Ebola virus transmission through the application of novel fractal–fractional operators with various kernel functions. A significant application of fractional calculus lies in the study of heat transfer in porous media. The fractional heat transfer equation provides a more precise and comprehensive model for heat transport in porous materials compared to the traditional heat transfer equation. Notably, researchers have devoted considerable attention to the study of fractals and fractional calculus in this context. This field has significant potential to improve our understanding of heat transfer in porous media, as demonstrated by numerous studies. The most notable applications of fractal and fractional theories are in mass and heat transfer processes in porous materials. Moreover, fractal theory provides an effective framework for exploring transport mechanisms, such as fluid flow in tree-like networks. A fractal model for capillary flow

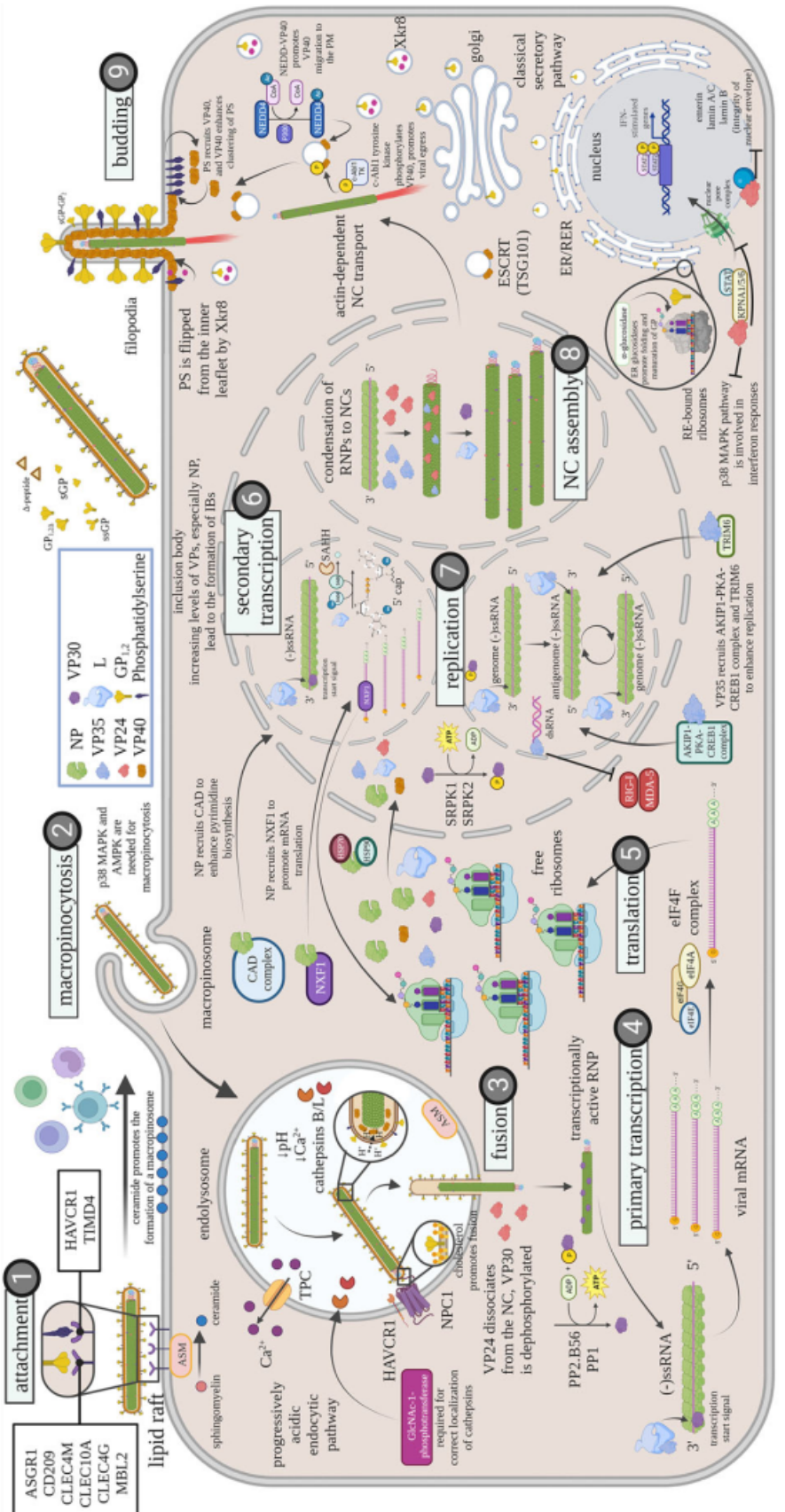

Fig. 1 Illustration of the dynamics of the Ebola virus life cycle. The process begins with virus attachment (1), mediated by cellular receptors and lipid raft domains, followed by macropinocytosis (2) for cellular entry. Within the endolysosome, fusion (3) is facilitated by cathepsins and cholesterol, enabling the release of the nucleocapsid. Subsequent steps include primary transcription (4), translation of viral proteins (5), and secondary transcription (6), leading to the synthesis of viral genomes and structural proteins. Replication (7) generates progeny genomes, which assemble into nucleocapsids (NC assembly, (8)). Finally, the virus buds from the host cell membrane (9), utilizing actin-dependent transport and the ESCRT machinery. Key host factors and signaling pathways influencing these stages are highlighted adapted from Ref. 6.

through a single tortuous capillary with roughened surfaces in fibrous porous media developed by Xiao *et al.*[28] An analytical model for permeability of fractal tree-like branched networks composed of converging-diverging capillaries was presented by Tu *et al.*[29] Li *et al.*[30] assessed a fractal analysis of dimensionless permeability and Kozeny–Carman constant of spherical granular porous media with randomly distributed tree-like branching networks. A fractal analytical model for Kozeny–Carman constant and permeability of roughened porous media composed of particles and converging-diverging capillaries developed by Xiao *et al.*[31] Liang *et al.*[32] investigated an analytical model for the transverse permeability of gas diffusion layer with electrical double layer effects in proton exchange membrane fuel cells. Long *et al.*[33] developed a analysis of crack problems in multilayered elastic medium by a consecutive stiffness method. Xiao *et al.*[34] used fractal study for nucleate pool boiling heat transfer of nanofluids. The author of Ref. 35 studied the prediction of heat transfer of nanofluid on critical heat flux based on fractal geometry. Xiao *et al.*[36] presented the analysis of convection heat transfer mechanism in nanofluids. Xiao *et al.*[37] used the fractal theory to investigate the subcooled pool boiling heat transfer in fractal nanofluids: A novel analytical model. Wang *et al.*[38] presented the fastest capillary flow in root-like networks under gravity. Several studies have utilized fractional-order models to describe the spread of infectious diseases; however, these approaches often neglect the fractal geometry of biological systems. The application of fractal derivatives allows for the integration of both spatial complexity and temporal memory effects, making it a more robust tool for understanding Ebola virus dynamics. Unlike existing models, the proposed fractal derivative framework captures the non-local and scale-invariant properties of the Ebola virus transmission dynamics. This novel approach provides a more realistic representation of the disease's progression and potential control strategies. The mentioned disease has been studied very well by using mathematical models, we refer to Refs. 39, 40, 41.

An extensive analysis of the model is conducted, including the derivation of the basic reproduction number ($\mathcal{R}_0$), positivity, and boundedness. Stability of equilibrium points is examined using the Routh–Hurwitz criteria, while Ulam–Hyers stability is assessed to ensure the robustness of the system. Existence and uniqueness of solutions are rigorously analyzed using fixed-point theorems, including Leray–Schauder and Banach's results. Sensitivity analyzes are performed to investigate the influence of key parameters on the model's behavior. To support the theoretical framework, numerical simulations are carried out using the Adams–Bashforth approximation method and an interpolation-based technique. Graphical illustrations are provided to depict the dynamics of the proposed model under various scenarios. The remainder of this paper is structured as follows: Section 2 introduces the foundational concepts of fractional calculus. Section 3 presents the primary findings, including theoretical and numerical analyses of the model. Section 4 discusses numerical simulations, and Sec. 5 concludes with remarks on the study's implications and future directions.

Figure 2 illustrates Ebola virus transmission dynamics within a population.

2. PRELIMINARIES

In this section, we recall some fundamental concepts and definitions that form the mathematical foundation of the proposed framework.

Definition 1 (Ref. 19). The fractal–fractional derivative in the Atangana–Baleanu–Caputo (ABC) sense, with fractional order $a \in (0,1]$ and fractal order $b \in (0,1]$, is defined for a function $G \in C[0,T]$ as follows:

$$ {}^{\mathrm{ABC}}_{0}\mathcal{D}_t^{a,b}(G(t)) = \frac{B(a)}{1-a}\frac{d}{dt^b}\int_0^t E_a\left[-a\frac{(t-\tau)^a}{1-a}\right] \times G(\psi)\,d\psi, \tag{1}$$

where $B(a)$ is a normalization function defined as

$$B(a) = 1 - a + \frac{a}{\Gamma(a)}.$$

Additionally, for $G \in L[0,T]$, the fractal–fractional integral in the Atangana–Baleanu sense, with fractional order $a \in (0,1]$ and fractal order $b \in (0,1]$, is given by

$$ {}^{\mathrm{ABC}}_{0}I_t^{a,b}(G(t)) = \frac{(1-a)\,b\,t^{b-1}}{B(a)}\,G(t) + \frac{a\,b}{\Gamma(a)\,B(a)} \times \int_0^t \psi^{\,b-1}(t-\psi)^{\,a-1}G(\psi)\,d\psi. \tag{2}$$

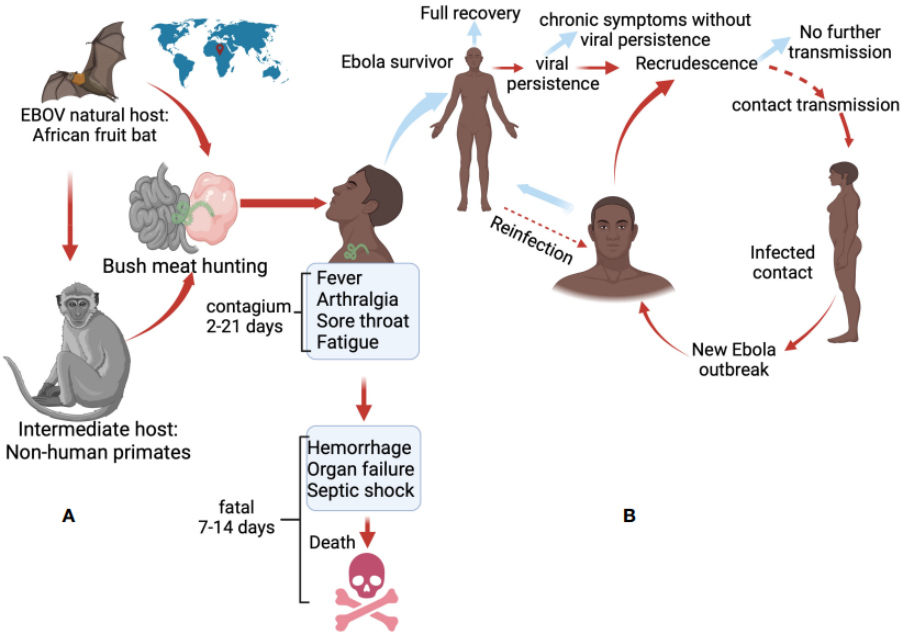

Fig. 2 Schematic representation of Ebola virus transmission dynamics within a population. The diagram illustrates the transmission pathways involving natural hosts (e.g. African fruit bats), intermediate hosts (e.g. non-human primates), and humans. Key stages of the infection, including symptom progression, recovery, reinfection, and potential outbreak cycles, are depicted. The figure highlights the zoonotic nature of the Ebola virus and its epidemiological impact on human populations.[6]

Definition 2 (Ref. 26). The ABC derivative exhibits Mittag-Leffler memory, as it incorporates the Mittag-Leffler function with parameter a, defined as

$$B_a(t) = \sum_{j=0}^{\infty} \frac{t^j}{\Gamma(aj+1)}, \quad a > 0. \tag{3}$$

This property ensures that the ABC derivative captures the long-term memory effects characteristic of fractional systems.

Lemma 3 (Ref. 26). *Let* $h \in L[0,T]$ *and* $h(0) = 0$. *The solution to the following initial value problem*:

$${}_0^{ABC}\mathcal{D}_t^{a,b}(G(t)) = h(t), \quad G(0) = G_0$$

is given by

$$G(t) = G_0 + \frac{(1-a)bt^{b-1}}{B(a)}h(t) + \frac{ab}{\Gamma(a)B(a)} \times \int_0^t \psi^{b-1}(t-\psi)^{a-1}h(\psi)\,d\psi. \tag{4}$$

These definitions and results establish the foundational tools necessary for the development and analysis of the fractal–fractional mathematical framework used in this study.

3. MAIN RESULTS

This section presents the key theoretical results of our proposed model.

3.1. Model Formulation

The transmission dynamics of the Ebola virus involve interactions among humans, domestic animals, and wild animals, all of which can act as potential reservoirs for infection. Motivated by the insights gained from previous research, we extend the framework proposed in Ref. 3 by incorporating additional complexities to better capture these interactions. The revised model, often referred to as the *SVEIHR* model, categorizes the total population into six distinct epidemiological compartments:

- $\mathcal{S}(t)$: The susceptible population at time t, representing individuals who have not yet been infected but are at risk of exposure.
- $\mathcal{V}(t)$: The vaccinated population consists of individuals protected through immunization.
- $\mathcal{E}(t)$: The exposed population, representing individuals who have been exposed to the virus but are not yet infectious.
- $\mathcal{I}(t)$: The infected population, which includes individuals actively carrying and potentially transmitting the virus at time t.

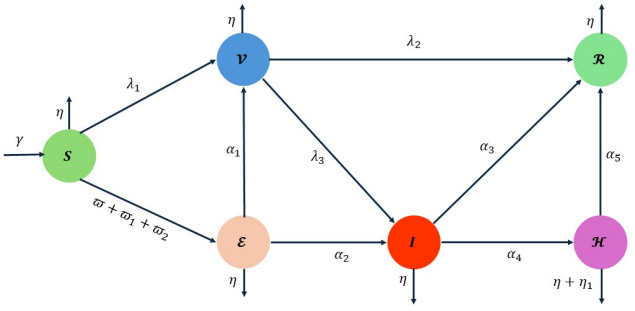

Fig. 3 Flowchart illustrating the compartments and transitions within the *SVEIHR* model for EVD. The diagram depicts the movement of individuals between the susceptible ($\mathcal{S}$), vaccinated ($\mathcal{V}$), exposed ($\mathcal{E}$), infected ($\mathcal{I}$), hospitalized ($\mathcal{H}$), and recovered ($\mathcal{R}$) compartments.

- $\mathcal{H}(t)$: The hospitalized population, consisting of individuals receiving treatment in medical facilities.
- $\mathcal{R}(t)$: The recovered population, representing individuals who have survived the infection and gained immunity, thus no longer susceptible to reinfection.

The compartmentalization of the population into these six groups provides a structured framework for analyzing the progression and control of the disease. Building on this model, we aim to enhance its analytical capabilities by employing a fractal–fractional approach within the Atangana–Baleanu sense. This advanced mathematical framework allows us to capture the intricate dynamics of the Ebola virus transmission, incorporating memory effects and complex spatial structures that are often inherent in real-world epidemiological systems. The *SVEIHR* model will provide deeper insights into the interplay of vaccination, exposure, and recovery, thereby aiding in the development of more effective strategies for disease control and prevention.

$$\begin{cases} {}^{\mathcal{FFM}}\mathcal{D}_t^{a,b}\mathcal{S}(t) = \gamma - (\varpi_1+\varpi_2+\varpi_3)\mathcal{S}\mathcal{E} \\ \qquad\qquad - (\lambda_1+\eta)\mathcal{S}, \\ {}^{\mathcal{FFM}}\mathcal{D}_t^{a,b}\mathcal{E}(t) = (\varpi_1+\varpi_2+\varpi_3)\mathcal{S}\mathcal{E} \\ \qquad\qquad - (\alpha_1+\alpha_2+\eta)\mathcal{E}, \\ {}^{\mathcal{FFM}}\mathcal{D}_t^{a,b}\mathcal{V}(t) = \lambda_1\mathcal{S} + \alpha_1\mathcal{E} - (\lambda_2+\lambda_3+\eta)\mathcal{V}, \\ {}^{\mathcal{FFM}}\mathcal{D}_t^{a,b}\mathcal{I}(t) = \alpha_2\mathcal{E} + \lambda_3\mathcal{V} - (\alpha_3+\alpha_4+\eta)\mathcal{I}, \\ {}^{\mathcal{FFM}}\mathcal{D}_t^{a,b}\mathcal{H}(t) = \alpha_4\mathcal{I} - (\alpha_5+\eta+\eta_1)\mathcal{H}, \\ {}^{\mathcal{FFM}}\mathcal{D}_t^{a,b}\mathcal{R}(t) = \lambda_2\mathcal{V} + \alpha_3\mathcal{I} + \alpha_5\mathcal{H} - \eta\mathcal{R}, \end{cases} \tag{5}$$

Table 1 Nomenclature and Physical Interpretation of Parameters in the *SVEIHR* Model (Eq. (5)).

Nomenclature	Physical Meaning
γ	Recruitment rate into the susceptible population, $\mathcal{S}(t)$
η	Natural mortality rate
η_1	Infection fatality rate
ϖ_1	Infection rate from $\mathcal{S}(t)$ to $\mathcal{E}(t)$ due to wild animals
ϖ_2	Infection rate from $\mathcal{S}(t)$ to $\mathcal{E}(t)$ due to human activity
ϖ_3	Infection rate from $\mathcal{S}(t)$ to $\mathcal{E}(t)$ due to domestic animals
λ_1	Rate of transition from susceptible individuals to vaccinated individuals
λ_2	Rate of transition from vaccinated individuals to recovered individuals
λ_3	Rate of transition from vaccinated individuals to infected individuals
α_1	Rate of transition from exposed individuals to vaccinated individuals
α_2	Rate of progression from $\mathcal{E}(t)$ (exposed) to $\mathcal{I}(t)$ (infected)
α_3	Rate of recovery from $\mathcal{I}(t)$ (infected) to $\mathcal{R}(t)$ (recovered)
α_4	Rate of hospitalization from $\mathcal{I}(t)$ (infected) to $\mathcal{H}(t)$ (hospitalized)
α_5	Rate of recovery from $\mathcal{H}(t)$ (hospitalized) to $\mathcal{R}(t)$ (recovered)

along with initial condition: $\mathcal{S}(0) = \mathcal{S}_0 \geq 0$, $\mathcal{E}(0) = \mathcal{E}_0 \geq 0$, $\mathcal{V}(0) = \mathcal{V}_0 \geq 0$, $\mathcal{I}(0) = \mathcal{I}_0 \geq 0$, $\mathcal{H}(0) = \mathcal{H}_0 \geq 0$, $\mathcal{R}(0) = \mathcal{R}_0 \geq 0$, the parameters are defined in Table 1.

3.2. Non-Negativity and Boundedness of the Model

Theorem 3.1. *Let the initial conditions of the system* (5) *be non-negative. Then, the solutions of the system* (5) *remain non-negative for all* $t > 0$.

Proof. We define $\Pi = \sup\{t > 0 \,|\, \mathcal{S}(t) \geq 0, \mathcal{E}(t) \geq 0, \mathcal{V}(t) \geq 0, \mathcal{I}(t) \geq 0, \mathcal{H}(t) \geq 0, \mathcal{R}(t) \geq 0\}$. Clearly, $\Pi > 0$ since $\mathcal{S}(0) > 0$ by assumption.

$$\begin{aligned} {}^{\mathcal{FFM}}\mathcal{D}_t^{a,b}\mathcal{S}(t) &= \gamma - (\varpi_1+\varpi_2+\varpi_3)\mathcal{S}\mathcal{E} \\ &\quad -(\lambda_1+\eta)\mathcal{S}, \\ {}^{\mathcal{FFM}}\mathcal{D}_t^{a,b}\mathcal{S}(t) &+ ((\varpi_1+\varpi_2+\varpi_3)\mathcal{E} \\ &\quad +(\lambda_1+\eta))\mathcal{S} \geq 0. \end{aligned} \tag{6}$$

By determining an integrating factor, we have

$$\mathcal{S}e^{(\lambda_1+\eta)t+\int_0^t(\varpi_1+\varpi_2+\varpi_3)\mathcal{E}dt)} \geq C,$$

where C is a constant determined by initial conditions. Solving this inequality with $\mathcal{S}(0) = \mathcal{S}_0$ and $C = \mathcal{S}(0)$, we get

$$\mathcal{S} \geq \mathcal{S}_0 e^{-((\lambda_1+\eta)t+\int_0^t(\varpi_1+\varpi_2+\varpi_3))\mathcal{E}dt)}.$$

In the inequality above $\mathcal{S}(0) > 0$,

$$e^{-((\lambda_1+\eta)t+\int_0^t(\varpi_1+\varpi_2+\varpi_3))\mathcal{E}dt)} \geq 0.$$

Since $\mathcal{S}_0 > 0$ and the exponential term is non-negative, it follows that $\mathcal{S}(t) > 0$ for all $t > 0$. Similarly, consider the evolution of $\mathcal{R}(t)$

$$\begin{aligned} {}^{\mathcal{FFM}}\mathcal{D}_t^{a,b}\mathcal{R}(t) &= \lambda_2\mathcal{V} + \alpha_3\mathcal{I} + \alpha_5\mathcal{H} - \eta\mathcal{R} \\ &\geq -\eta\mathcal{R}. \end{aligned}$$

$$ {}^{\mathcal{FFM}}\mathcal{D}_t^{a,b}\mathcal{R}(t) + \eta\mathcal{R} \geq 0. \tag{7}$$

As a result of the integrating factor and applying the initial conditions $\mathcal{R}(0) = \mathcal{R}_0$, we obtain

$$\mathcal{R}e^{(\eta)t} \geq C, \quad \mathcal{R} = \mathcal{R}_0 e^{-(\eta)t} \geq 0.$$

Since $\mathcal{R}_0 \geq 0$ and $e^{-\eta t} \geq 0$, we conclude that $\mathcal{R}(t) \geq 0$ for all $t \geq 0$. Following similar arguments for all state variables, we deduce that the solutions of (5) remain non-negative for all $t \geq 0$. This property ensures the positivity and physical relevance of the proposed model. □

3.3. Disease-Free Equilibrium Point ($\mathcal{X}_0$)

The disease-free equilibrium (DFE) point is denoted via $\mathcal{X}_0$, where $\mathcal{X}_0 = (\mathcal{S}_0, \mathcal{E}_0, \mathcal{V}_0, \mathcal{I}_0, \mathcal{H}_0, \mathcal{R}_0)$. This aspect will occurs when $\mathcal{R}_0 < 1$. To analyze this aspect, we site $\mathcal{E}(t) = \mathcal{V}(t) = \mathcal{I}(t) = \mathcal{H}(t) = \mathcal{R}(t) = 0$, with $\mathcal{S}_0 = \frac{\gamma}{\lambda_1+\eta}$. Thus, the DFE element of system (5) is given by

$$\begin{aligned} \mathcal{X}_0 &= (\mathcal{S}_0, \mathcal{E}_0, \mathcal{V}_0, \mathcal{I}_0, \mathcal{H}_0, \mathcal{R}_0) \\ &= \left(\frac{\gamma}{\lambda_1+\eta}, 0, 0, 0, 0, 0\right). \end{aligned} \tag{8}$$

3.4. The Endemic Equilibrium Point ($\mathcal{X}_1$)

The endemic equilibrium point (EEP) is denoted via $\mathcal{X}_1$; where the EEP for model (5) is equivalent to 0 and replacing all elements $(\mathcal{S}, \mathcal{E}, \mathcal{V}, \mathcal{I}, \mathcal{H}, \mathcal{R})$ with

$$(\mathcal{S}^\star, \mathcal{E}^\star, \mathcal{V}^\star, \mathcal{I}^\star, \mathcal{H}^\star, \mathcal{R}^\star)$$

and once simplification and rearrangement are complete, we'll obtain the EEPs $\mathcal{X}_1$:

$$\begin{cases} \mathcal{S}^\star = \dfrac{\gamma}{\lambda_1+\eta}\left(\dfrac{1}{\mathcal{R}_0}\right), \\ \mathcal{E}^\star = \dfrac{p_1\,\gamma - p_2\,p_3}{p_1\,p_3}, \\ \mathcal{V}^\star = \dfrac{p_1\,\alpha_1\,\gamma - p_2\,p_3\,\alpha_1 + {p_3}^2\lambda_1}{p_1\,p_3\,p_4}, \\ \mathcal{I}^\star = \dfrac{\begin{array}{c} p_1\,p_4\,\alpha_2\,\gamma + p_1\,\alpha_1\,\lambda_3\,\gamma - p_2\,p_3\,p_4\,\alpha_2 \\ -p_2\,p_3\,\alpha_1\,\lambda_3 + {p_3}^2\lambda_1\,\lambda_3 \end{array}}{p_1\,p_3\,p_4\,p_5}, \\ \mathcal{H}^\star = \dfrac{\begin{array}{c} \alpha_4\,({p_3}^2\lambda_1\,\lambda_3 - p_2\,(p_4\,\alpha_2 + \alpha_1\,\lambda_3)p_3 \\ +p_1\,\gamma\,(p_4\,\alpha_2 + \alpha_1\,\lambda_3)) \end{array}}{p_1\,p_3\,p_4\,p_5\,p_6}, \\ \mathcal{R}^\star = \dfrac{\begin{array}{c} (\lambda_1\,q_1{p_3}^2 - p_2\,q_2p_3 + p_1\,\gamma\,q_3)\alpha_6 \\ +\alpha_4\,(q_4 - p_2\,q_5p_3 + p_1\,\lambda\,q_5)\alpha_5 \end{array}}{p_3\,p_1\,p_4\,p_5\,\alpha_6\,\eta}, \end{cases} \tag{9}$$

where

$$\begin{aligned} p_1 &= (\varpi_1 + \varpi_2 + \varpi_3), \\ p_2 &= (\lambda_1 + \eta), \\ p_3 &= (\alpha_1 + \alpha_2 + \eta), \\ p_4 &= (\lambda_2 + \lambda_3 + \eta), \\ p_5 &= (\alpha_3 + \alpha_4 + \eta), \\ p_6 &= (\alpha_5 + \eta + \eta_1). \\ q_1 &= (p_5\,\lambda_2 + \alpha_3\,\lambda_3), \\ q_2 &= (p_4\,\alpha_2\,\alpha_3 + p_5\,\alpha_1\,\lambda_2 + \alpha_1\,\alpha_3\,\lambda_3), \\ q_3 &= (p_4\,\alpha_2\,\alpha_3 + p_5\,\alpha_1\,\lambda_2 + \alpha_1\,\alpha_3\,\lambda_3), \\ q_4 &= \lambda_1\,\lambda_3\,{p_3}^2, \\ q5 &= (p_4\,\alpha_2 + \alpha_1\,\lambda_3). \end{aligned}$$

3.5. The Basic Reproductive Number $\mathcal{R}_0$

$$\mathcal{F} = \begin{pmatrix} (\varpi_1 + \varpi_2 + \varpi_3)\mathcal{S}\mathcal{E} \\ 0 \\ 0 \\ 0 \end{pmatrix},$$

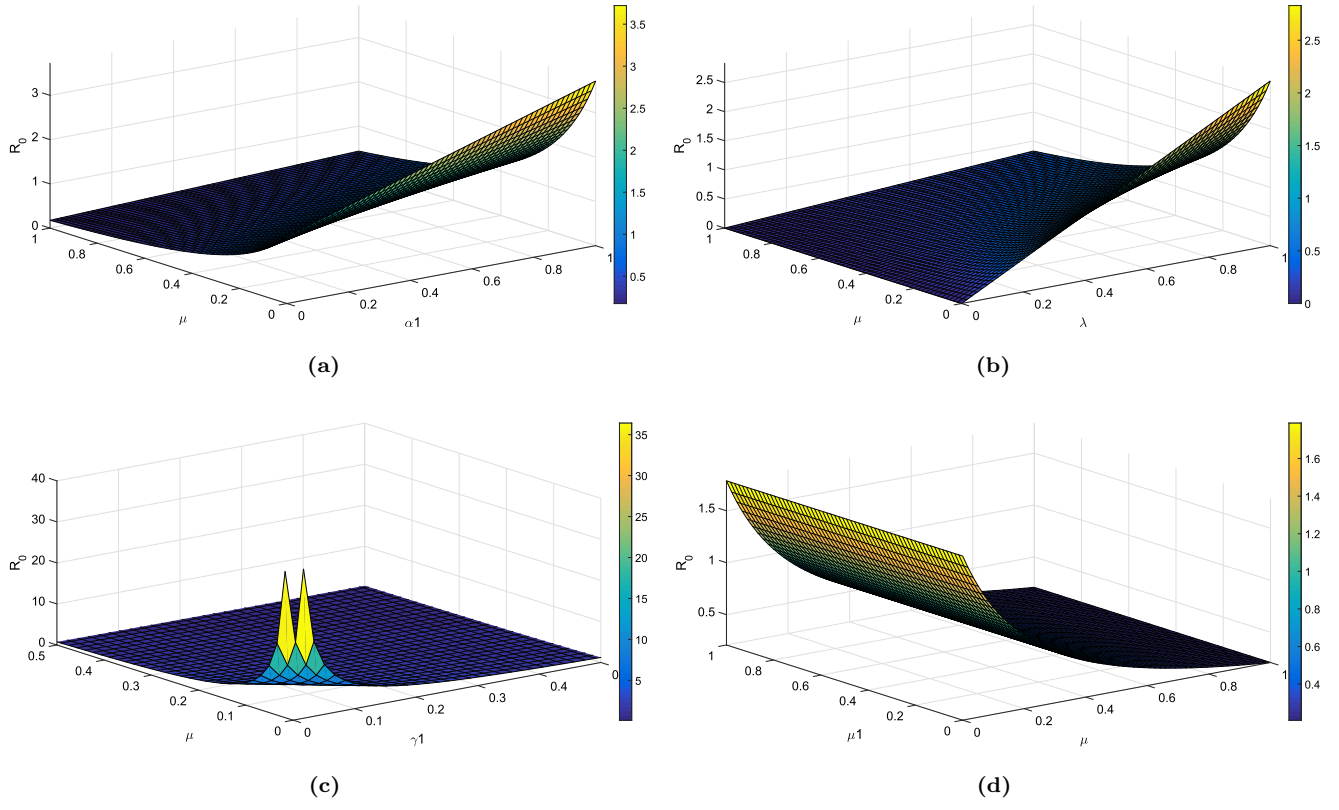

Fig. 4 Graphical profile with 3D images of Reproduction number against various parameters.

$$\mathcal{V} = \begin{pmatrix} (\alpha_1 + \alpha_2 + \eta)\mathcal{E} \\ -\lambda_1 S - \alpha_1 \mathcal{E} + (\lambda_2 + \lambda_3 + \eta)\mathcal{V} \\ -\alpha_2 E - \lambda_3 \mathcal{V} + (\alpha_3 + \alpha_4 + \eta) I \\ -\alpha_4 I + (\alpha_5 + \eta + \eta_1)\mathcal{H} \end{pmatrix}.$$

By computing the Jacobian of the above using $(\mathcal{X}_0)$, we obtain

$$\mathcal{F}^* = \begin{pmatrix} (\varpi_1 + \varpi_2 + \varpi_3)S & 0 & 0 & 0 \\ 0 & 0 & 0 & 0 \\ 0 & 0 & 0 & 0 \\ 0 & 0 & 0 & 0 \end{pmatrix},$$

$$\mathcal{V}^* = \begin{pmatrix} \alpha_1 + \alpha_2 + \eta & 0 & 0 & 0 \\ -\alpha_1 & \lambda_2 + \lambda_3 + \eta & 0 & 0 \\ -\alpha_2 & -\lambda_3 & \alpha_3 + \alpha_4 + \eta & 0 \\ 0 & 0 & -\alpha_4 & \alpha_5 + \eta + \eta_1 \end{pmatrix}.$$

According to Refs. 39 and 40, the threshold quantity $\mathcal{R}_0$ is the spectral radius ϱ of the matrix $\mathcal{F}^* \mathcal{V}^{*-1}$, and it is

$$\mathcal{R}_0 = \varrho(\mathcal{F}^* \mathcal{V}^{*-1}) = \frac{(\varpi_1 + \varpi_2 + \varpi_3)\gamma}{(\alpha_1 + \alpha_2 + \eta)(\lambda_1 + \eta)}. \quad (10)$$

Figure 4 illustrates the parametric sensitivity of the basic reproduction number, $\mathcal{R}_0$, under varying model parameters. Figure 4a shows the influence of ϖ and η on $\mathcal{R}_0$; Fig. 4b shows the interplay between γ and η in determining $\mathcal{R}_0$; Fig. 4c shows the effect of λ_1 and η on $\mathcal{R}_0$; and Fig. 4d shows the combined impact of η and η_1 on $\mathcal{R}_0$. The above figure shows that $\mathcal{R}_0$ is directly proportional to γ and ϖ_1 and inversely proportional to η. Also $\mathcal{R}_0$ is directly proportional to enumerator and inversely proportional to the denominator.

3.6. Local Stability Analysis

Theorem 3.2. *The proposed model* (5) *is locally asymptotically stable* (*LAS*) *at the disease-free equilibrium point* (*DFEP*) $\mathcal{X}_0$, *which lies within the set* Π, *if* $\mathcal{R}_0 < 1$. *Conversely, if* $\mathcal{R}_0 > 1$, *the system becomes unstable.*

Proof. The Jacobian matrix of system (5) evaluated at the DFEP $\mathcal{X}_0$ is given as

$$\mathcal{J}(\mathcal{X}_0) = \begin{pmatrix} -b_1 & 0 & -\frac{\gamma b_3}{b_1} & 0 & 0 & 0 \\ 0 & 0 & \frac{\gamma b_3}{b_1} - b_4 & 0 & 0 & 0 \\ \lambda_1 & -b_2 & \alpha_1 & 0 & 0 & 0 \\ 0 & \lambda_3 & \alpha_2 & -b_5 & 0 & 0 \\ 0 & 0 & 0 & \alpha_4 & -b_6 & 0 \\ 0 & \lambda_2 & 0 & \alpha_3 & \alpha_5 & -\eta \end{pmatrix}.$$

Here, the parameters are defined as follows:

$$b_1 = \lambda_1 + \eta, \qquad b_2 = \lambda_2 + \lambda_3 + \eta,$$
$$b_3 = \varpi_1 + \varpi_2 + \varpi_3, \qquad b_4 = \alpha_1 + \alpha_2 + \eta,$$
$$b_5 = \alpha_3 + \alpha_4 + \eta. \qquad b_6 = \alpha_5 + \eta + \eta_1.$$

The eigenvalues of the Jacobian matrix are as follows:

$$\Lambda_1 = -\eta,$$
$$\Lambda_2 = -b_6 = -(\alpha_5 + \eta + \eta_1),$$
$$\Lambda_3 = -b_5 = -(\alpha_3 + \alpha_4 + \eta).$$

Since the matrix is lower triangular, the eigenvalues are located on the diagonal (Table 2). The reduced matrix becomes:

$$\mathcal{J}(\mathcal{P}_1) = \begin{pmatrix} -b_1 & 0 & -\frac{\gamma b_3}{b_1} \\ 0 & -b_4 & \frac{\gamma b_3}{b_1} - b_4 \\ \lambda_1 & -b_2 & \alpha_1 \end{pmatrix}.$$

The characteristic polynomial at $\mathcal{J}(\mathcal{X}_1)$ is given by

$$\det(\mathcal{J}(\mathcal{X}_1) - \Lambda I) = 0,$$

where Λ represents the eigenvalue and I is the 3×3 identity matrix. This determinant expands as

$$\det(\mathcal{J}(\mathcal{X}_1) - \Lambda I) = \begin{vmatrix} -b_1 - \Lambda & 0 & -\frac{\gamma b_3}{b_1} \\ 0 & -\Lambda & \frac{\gamma b_3}{b_1} - b_4 \\ \lambda_1 & -b_2 & \alpha_1 - \Lambda \end{vmatrix} = 0.$$

Simplifying the determinant yields the characteristic polynomial:

$$\rho_0 \Lambda^3 + \rho_1 \Lambda^2 + \rho_2 \Lambda + \rho_3 = 0, \qquad (11)$$

where the coefficients are given by

$$\rho_0 = 1,$$
$$\rho_1 = b_1 + \alpha_1,$$
$$\rho_2 = (b_2 + \lambda_1) b_4 \mathcal{R}_0 + b_2 b_4 - b_1 \alpha_1,$$
$$\rho_3 = b_1 b_2 b_4 (1 - \mathcal{R}_0).$$

Using the Routh–Hurwitz criterion to analyze polynomial (11), the Routh–Hurwitz table is constructed as follows.

Based on the Routh–Hurwitz criterion, the system is LAS if all the coefficients of the first column (C_1) are positive. Thus, the system is LAS if

$$\frac{\rho_1 \rho_2 - \rho_0 \rho_3}{\rho_1} \geq 0, \quad \rho_1 \rho_2 - \rho_0 \rho_3 \geq 0,$$
$$\rho_1 \rho_2 \geq \rho_3, \quad \rho_1 \rho_2 \geq b_1 b_2 b_4 (1 - \mathcal{R}_0).$$

If these conditions are not satisfied, the system becomes unstable. □

3.7. Endemic Equilibrium Point

The EEP of the system is analyzed in this section and is represented as

$$\mathcal{X}_1 = (\mathcal{S}^\star, \mathcal{E}^\star, \mathcal{V}^\star, \mathcal{I}^\star, \mathcal{H}^\star, \mathcal{R}^\star),$$

where $\mathcal{S}^\star$, $\mathcal{E}^\star$, $\mathcal{V}^\star$, $\mathcal{I}^\star$, $\mathcal{H}^\star$, and $\mathcal{R}^\star$ denote the steady-state values of the susceptible, exposed, vaccinated, infectious, hospitalized, and recovered populations, respectively.

Theorem 3.3. *The proposed system* (5) *is LAS at the EEP* $\mathcal{X}_1$ *if* $\mathcal{R}_0 > 1$.

Proof. The Jacobian matrix for framework (5) at EEP $\mathcal{X}_1$ is

$$\mathcal{J}(\mathcal{X}_1) = \begin{pmatrix} -p_1 \mathcal{E}^\star - p_2 & -p_1 \mathcal{S}^\star & 0 & 0 & 0 & 0 \\ p_1 \mathcal{E}^\star & p_1 \mathcal{S}^\star - p_3 & 0 & 0 & 0 & 0 \\ \lambda_1 & \alpha_1 & -p_4 & 0 & 0 & 0 \\ 0 & \alpha_2 & \lambda_3 & -b_5 & 0 & 0 \\ 0 & 0 & 0 & \lambda_4 & -b_6 & 0 \\ 0 & 0 & \lambda_2 & \alpha_3 & \alpha_5 & -\eta \end{pmatrix},$$

Table 2 Routh–Hurwitz Table.

Degree	C_1	C_2
Λ^3	ρ_0	ρ_2
Λ^2	ρ_1	ρ_3
Λ^1	$\frac{\rho_1 \rho_2 - \rho_0 \rho_3}{\rho_1}$	0
Λ^0	ρ_3	0

where

$$\mathcal{X}_1 = (\varpi_1 + \varpi_2 + \varpi_3), \quad p_2 = (\lambda_1 + \eta), \qquad p_3 = (\alpha_1 + \alpha_2 + \eta), \quad p_4 = (\lambda_2 + \lambda_3 + \eta),$$
$$p_5 = (\alpha_3 + \alpha_4 + \eta), \quad p_6 = (\alpha_5 + \eta + \eta_1).$$

The essential polynomial at $\mathcal{X}_1$ is expressed as $\det(\mathcal{J} - \gamma I) = 0$, where γ represents the eigenvalue and I is 6×6 diagonal matrix, Hence

$$|\mathcal{J} - \gamma I| = \begin{vmatrix} -p_1\mathcal{E}^\star - p_2 - \gamma & -p_1\mathcal{S}^\star & 0 & 0 & 0 & 0 \\ p_1\mathcal{E}^\star & p_1\mathcal{S}^\star - p_3 - \gamma & 0 & 0 & 0 & 0 \\ \lambda_1 & \alpha_1 & -p_4 - \gamma & 0 & 0 & 0 \\ 0 & \alpha_2 & \lambda_3 & -p_5 - \gamma & 0 & 0 \\ 0 & 0 & 0 & \alpha_4 & -p_6 - \gamma & 0 \\ 0 & 0 & \lambda_2 & \alpha_3 & \alpha_5 & -\eta - \gamma \end{vmatrix} = 0.$$

Simplifying the characteristic polynomial (i.e. making the characteristic equation) and solving for γ gives

$$\begin{aligned} \gamma_1 &= -\eta, \\ \gamma_2 &= -p_6 = -(\alpha_5 + \eta + \eta_1), \\ \gamma_3 &= -p_5 = -(\alpha_3 + \alpha_4 + \eta), \\ \gamma_4 &= -p_4 = -(\lambda_2 + \lambda_3 + \eta). \end{aligned} \tag{12}$$

The characteristic equation $\gamma^2 + (p_1(\mathcal{E}^\star - \mathcal{S}^\star) + p_2 + p_3)\gamma + p_1p_2(1 + \mathcal{E}^\star - \mathcal{S}^\star) = 0$ consists entirely of positive terms, which ensures that all its roots are negative. Thus, $\gamma_{5,6} < 0$ concluding the proof. □

3.8. Sensitivity Analysis of $\mathcal{R}_0$

$\mathcal{R}_0$ is interpreted by the sensitivity analysis. It assists in identifying the key parameters accountable for direct spread and control of the illness. The major reason for the framework is to oversee connection of the key factors associated with the $\mathcal{R}_0$. To assess the indices of sensitivity, we will utilize the rule employed by Khan *et al.*[41]

$$\mathcal{Q}_y^{\mathcal{R}_0} = \frac{y}{\mathcal{R}_0}\left[\frac{\partial \mathcal{R}_0}{\partial y}\right], \tag{13}$$

where $\zeta \in (\gamma, \varpi_1, \varpi_2, \varpi_3, \lambda_1, \alpha_1, \alpha_2, \eta)$. That appears in $\mathcal{R}_0 = \frac{\gamma(\varpi_1+\varpi_2+\varpi_3)}{(\alpha_1+\alpha_2+\eta)(\lambda_1+\eta)}$.

Using parameters values of Table 3, the sensitivity indices are presented by bar graphs in Fig. 5.

Differentiating equation (13) with respect to each of the above perimeter individually, we obtain:

$$\mathcal{Q}_\gamma^{\mathcal{R}_0} = \frac{\gamma}{\mathcal{R}_0}\left[\frac{\partial \mathcal{R}_0}{\partial \gamma}\right]$$

$$\begin{aligned} &= \frac{\partial}{\partial \gamma}\left(\frac{\gamma(\varpi_1 + \varpi_2 + \varpi_3)}{(\alpha_1 + \alpha_2 + \eta)(\lambda_1 + \eta)}\right) \\ &\quad \times \frac{\gamma(\lambda_1 + \eta)(\alpha_1 + \alpha_2 + \eta)}{\gamma(\varpi_1 + \varpi_2 + \varpi_3)} \\ &= \frac{(\varpi_1 + \varpi_2 + \varpi_3)}{(\alpha_1 + \alpha_2 + \eta)(\lambda_1 + \eta)} \\ &\quad \times \frac{\gamma(\alpha_1 + \alpha_2 + \eta)(\lambda_1 + \eta)}{\gamma(\varpi_1 + \varpi_2 + \varpi_3)} = 1, \end{aligned}$$

$$\mathcal{Q}_{\varpi_1}^{\mathcal{R}_0} = \frac{\varpi_1}{\mathcal{R}_0}\left[\frac{\partial \mathcal{R}_0}{\partial \varpi_1}\right] = 0.1521,$$

$$\mathcal{Q}_{\varpi_2}^{\mathcal{R}_0} = \frac{\varpi_2}{\mathcal{R}_0}\left[\frac{\partial \mathcal{R}_0}{\partial \varpi_2}\right] = 0.3547,$$

$$\mathcal{Q}_{\varpi_3}^{\mathcal{R}_0} = \frac{\varpi_3}{\mathcal{R}_0}\left[\frac{\partial \mathcal{R}_0}{\partial \varpi_3}\right] = 0.4931,$$

$$\mathcal{Q}_{\lambda_1}^{\mathcal{R}_0} = \frac{\lambda_1}{\mathcal{R}_0}\left[\frac{\partial \mathcal{R}_0}{\partial \lambda_1}\right] = -0.5389,$$

$$\mathcal{Q}_{\alpha_1}^{\mathcal{R}_0} = \frac{\alpha_1}{\mathcal{R}_0}\left[\frac{\partial \mathcal{R}_0}{\partial \alpha_1}\right] = -0.1721,$$

$$\mathcal{Q}_{\alpha_2}^{\mathcal{R}_0} = \frac{\alpha_2}{\mathcal{R}_0}\left[\frac{\partial \mathcal{R}_0}{\partial \alpha_2}\right] = -0.6551,$$

$$\mathcal{Q}_{\eta}^{\mathcal{R}_0} = \frac{\eta}{\mathcal{R}_0}\left[\frac{\partial \mathcal{R}_0}{\partial \eta}\right] = -0.2006.$$

The sensitivity analysis of the $\mathcal{R}_0$ in view of the given parameters is carried out both graphically and numerically. Here, γ, ϖ_1, ϖ_2, and ϖ_3 have a positive impact on $\mathcal{R}_0$, whereas α_1, α_2, η, and λ_1 have a negative impacts on $\mathcal{R}_0$. Amongst them, γ and α_2 are the most sensitive parameters.

Table 3 Ratio Allocate Parameters of the Framework (5) for the Imitation.

Parameter	Ratio (Per Day)	Source	Parameter	Ratio (Per Day)	Source
γ	0.06321	Ref. 3	λ_3	0.04123	Ref. 7
ϖ_1	0.01234	Ref. 3	α_1	0.02	assumed
ϖ_2	0.02877	Ref. 3	α_2	0.07613	Refs. 3 and 7
ϖ_3	0.04000	Ref. 3	α_3	0.04389	Ref. 3
η	0.02006	assumed	α_4	0.06	Ref. 5
λ_1	0.02345	Ref. 7	α_5	0.0629	Ref. 5
λ_2	0.05111	Ref. 7	η_1	0.0029	assumed

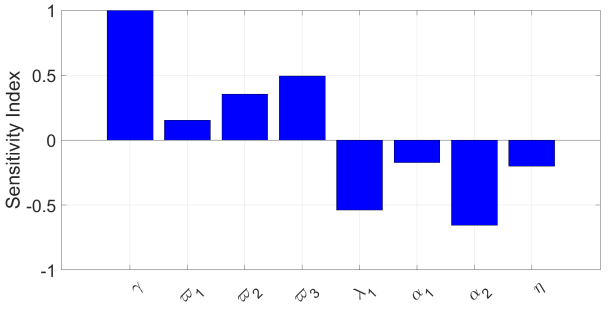

Fig. 5 Effect of parameters on $\mathcal{R}_0$.

3.9. Existence Results

Given that the integral is differentiable, we are able to express the suggested framework as: In this point, we validate the presence of at least one solution for the proposed considered system utilizing results regarding fixed point.

$$\begin{cases} {}^{\mathcal{FFM}}\mathcal{D}_t^{a,b}\mathcal{S}(t) = \gamma - (\varpi_1+\varpi_2+\varpi_3)\mathcal{S}\mathcal{E} \\ \qquad\qquad - (\lambda_1+\eta)\mathcal{S}, \\ {}^{\mathcal{FFM}}\mathcal{D}_t^{a,b}\mathcal{E}(t) = (\varpi_1+\varpi_2+\varpi_3)\mathcal{S}\mathcal{E} \\ \qquad\qquad - (\alpha_1+\alpha_2+\eta)\mathcal{E}, \\ {}^{\mathcal{FFM}}\mathcal{D}_t^{a,b}\mathcal{V}(t) = \lambda_1\mathcal{S}+\alpha_1\mathcal{E}-(\lambda_2+\lambda_3+\eta)\mathcal{V}, \\ {}^{\mathcal{FFM}}\mathcal{D}_t^{a,b}\mathcal{I}(t) = \alpha_2\mathcal{E}+\lambda_3\mathcal{V}-(\alpha_3+\alpha_4+\eta)\mathcal{I}, \\ {}^{\mathcal{FFM}}\mathcal{D}_t^{a,b}\mathcal{H}(t) = \alpha_4\mathcal{I}-(\alpha_5+\eta+\eta_1)\mathcal{H}, \\ {}^{\mathcal{FFM}}\mathcal{D}_t^{a,b}\mathcal{R}(t) = \lambda_2\mathcal{V}+\alpha_3\mathcal{I}+\alpha_5\mathcal{H}-\eta\mathcal{R}, \end{cases} \tag{14}$$

where

$$\begin{cases} \boldsymbol{B}_1(t,\mathcal{S},\mathcal{E},\mathcal{V},\mathcal{I},\mathcal{H},\mathcal{R}) \\ \qquad = \gamma-(\varpi_1+\varpi_2+\varpi_3)\mathcal{S}\mathcal{E}-(\lambda_1+\eta)\mathcal{S}, \\ \boldsymbol{B}_2(t,\mathcal{S},\mathcal{E},\mathcal{V},\mathcal{I},\mathcal{H},\mathcal{R}) \\ \qquad = (\varpi_1+\varpi_2+\varpi_3)\mathcal{S}\mathcal{E}-(\alpha_1+\alpha_2+\eta)\mathcal{E}, \\ \boldsymbol{B}_3(t,\mathcal{S},\mathcal{E},\mathcal{V},\mathcal{I},\mathcal{H},\mathcal{R}) \\ \qquad = \lambda_1\mathcal{S}+\alpha_1\mathcal{E}-(\lambda_2+\lambda_3+\eta)\mathcal{V}, \\ \boldsymbol{B}_4(t,\mathcal{S},\mathcal{E},\mathcal{V},\mathcal{I},\mathcal{H},\mathcal{R}) \\ \qquad = \alpha_2\mathcal{E}+\lambda_3\mathcal{V}-(\alpha_3+\alpha_4+\eta)\mathcal{I}, \\ \boldsymbol{B}_5(t,\mathcal{S},\mathcal{E},\mathcal{V},\mathcal{I},\mathcal{H},\mathcal{R}) \\ \qquad = \alpha_4\mathcal{I}-(\alpha_5+\eta+\eta_1)\mathcal{H}, \\ \boldsymbol{B}_5(t,\mathcal{S},\mathcal{E},\mathcal{V},\mathcal{I},\mathcal{H},\mathcal{R}) \\ \qquad = \lambda_2\mathcal{V}+\alpha_3\mathcal{I}+\alpha_5\mathcal{H}-\eta\mathcal{R}. \end{cases} \tag{15}$$

We can formulate the model (5) as

$$\begin{cases} {}^{\mathrm{FFM}}\mathcal{D}_t^a\psi(t) = bt^{b-1}\Pi(t,\psi(t)), \\ \psi(0)=\psi_0. \end{cases}$$

By replacing ${}_0^{ABR}\mathcal{D}_0^{a,b}$ by ${}_0^{ABC}\mathcal{D}_0^{a,b}$ and using non-integers integral, we obtain

$$\psi(t) = \psi(0) + \frac{bt^{b-1}(1-a)}{AB(a)}\Pi(t,\psi(t)) + \frac{ab}{AB(a)\Gamma(a)} \times \int_0^t \sigma^{b-1}(t-\sigma)^{b-1}\Pi(t,\psi(t))d\sigma,$$

where

$$\psi(t) = \begin{pmatrix} \mathcal{S}(t) \\ \mathcal{E}(t) \\ \mathcal{V}(t) \\ \mathcal{I}(t) \\ \mathcal{H}(t) \\ \mathcal{R}(t) \end{pmatrix}, \quad \psi(0) = \begin{pmatrix} \mathcal{S}(0) \\ \mathcal{E}(0) \\ \mathcal{V}(0) \\ \mathcal{I}(0) \\ \mathcal{H}(0) \\ \mathcal{R}(0) \end{pmatrix},$$

$$\Pi(t,\psi(t)) = \begin{pmatrix} \boldsymbol{B}_1(t,\mathcal{S},\mathcal{E},\mathcal{V},\mathcal{I},\mathcal{H},\mathcal{R}) \\ \boldsymbol{B}_2(t,\mathcal{S},\mathcal{E},\mathcal{V},\mathcal{I},\mathcal{H},\mathcal{R}) \\ \boldsymbol{B}_3(t,\mathcal{S},\mathcal{E},\mathcal{V},\mathcal{I},\mathcal{H},\mathcal{R}) \\ \boldsymbol{B}_4(t,\mathcal{S},\mathcal{E},\mathcal{V},\mathcal{I},\mathcal{H},\mathcal{R}) \\ \boldsymbol{B}_5(t,\mathcal{S},\mathcal{E},\mathcal{V},\mathcal{I},\mathcal{H},\mathcal{R}) \\ \boldsymbol{B}_6(t,\mathcal{S},\mathcal{E},\mathcal{V},\mathcal{I},\mathcal{H},\mathcal{R}) \end{pmatrix}.$$

In the context regarding fixed point theory, we introduce a Banach space defined as $\mathcal{C} = \mathcal{M} \times \mathcal{M} \times \mathcal{M} \times \mathcal{M} \times \mathcal{M}$, where $\mathcal{M} = [0, \tau]$ utilizing the norm

$$\|\psi\| = \max_{t\in[0,\tau]} |\mathcal{S}(t) + \mathcal{E}(t) + \mathcal{V}(t) + \mathcal{I}(t) + \mathcal{H}(t) + \mathcal{R}(t)|.$$

Define the operator $\Pi : \mathcal{C} \to \mathcal{C}$ as

$$\Pi(\psi)(t) = \psi(0) + \frac{bt^{b-1}(1-a)}{AB(a)}\Omega(t,\psi(t)) + \frac{ab}{AB(a)\Gamma(a)}\int_0^t \sigma^{b-1}(t-\sigma)^{b-1} \times \Omega(t,\psi(t))d\sigma. \quad (16)$$

Next, let's presume that the nonlinear function $\Omega(t, \psi(t))$ fulfills the ensuring growth and Lipschitz constraints:

- For every $\psi \in \mathcal{C}$, $\exists$ parameters $Q_\Omega > 0$ and $\mathcal{W}_\Omega$ in such a way that
$$|\Omega(t,\psi(t))| \le Q_\Omega|\psi(t)| + \mathcal{W}_\Omega. \quad (17)$$
- For each $\psi, \overline{\psi} \in \mathcal{C}$, $\exists$ constants $\mathcal{P}_\Omega > 0$ such that
$$|\Omega(t,\psi(t)) - \Omega(t,\overline{\psi}(t))| \le \mathcal{P}_\Omega|\psi(t) - \overline{\psi}(t)|. \quad (18)$$

Theorem 3.4. *Suppose the condition* (17) *holds. Let* $\Omega : [0,\tau] \times \mathcal{C} \to \mathcal{R}$ *be a continuous function. Therefore, the proposed model possesses at least one solution.*

Proof. Initially, we must demonstrate that the operator Π defined by (16) exhibits complete continuity. As Ω is continuous, it follows that Π is also continuous.

Let $\mathcal{M} = \{\psi \in \mathcal{C} : \|\psi\| \le \mathcal{R}, \mathcal{R} > 0\}$. Now for any $\psi \in \mathcal{C}$, we have

$$\begin{aligned}
|\Pi(\psi)| &= \max_{t\in[0,\tau]} \left|\psi(0) + \frac{bt^{b-1}(1-a)}{AB(a)}\Omega(t,\psi(t)) + \frac{ab}{AB(a)\Gamma(a)}\int_0^t \sigma^{b-1}(t-\sigma)^{b-1}\Omega(t,\psi(t))d\sigma\right| \\
&\le \psi(0) + \frac{bt^{b-1}(1-a)}{AB(a)}(Q_\Omega\|\psi\| + \mathcal{W}_\Omega) + \max_{t\in[0,\tau]} \times \frac{ab}{AB(a)\Gamma(a)}\int_0^t \sigma^{b-1}(t-\sigma)^{b-1}|\Omega(\sigma,\psi(\sigma))|d\sigma \\
&\le \psi(0) + \frac{bt^{b-1}(1-a)}{AB(a)}(Q_\Omega\|\psi\| + \mathcal{W}_\Omega) + \frac{ab}{AB(a)\Gamma(a)}(Q_\Omega\|\psi\| + \mathcal{W}_\Omega)t^{b-1}\mathcal{M}(a,b) \\
&\le \mathcal{R}.
\end{aligned}$$

Therefore, the operator Π is uniformly bounded, with $\mathcal{M}(a,b)$ denoting the beta function.

For equi-continuity of Π let us take $t_1 < t_2 \le \tau$ then consider,

$$\begin{aligned}
&|\Pi(\psi)(t_2) - \Pi(\psi)(t_1)| \\
&= \left|\left(\frac{bt_2^{b-1}(1-a)}{AB(a)}\Omega(t_2,\psi(t_2)) + \frac{ab}{AB(a)\Gamma(a)} \times \int_0^{t_2} \sigma^{b-1}(t_2-\sigma)^{b-1}\Omega(\sigma,\psi(\sigma))d\sigma\right)\right. \\
&\quad \left. - \left(\frac{bt_1^{b-1}(1-a)}{AB(a)}\Omega(t_1,\psi(t_1)) + \frac{ab}{AB(a)\Gamma(a)} \times \int_0^{t_1} \sigma^{b-1}(t_1-\sigma)^{b-1}\Omega(\sigma,\psi(\sigma))d\sigma\right)\right| \\
&\le \frac{bt_2^{b-1}(1-a)}{AB(a)}(Q_\Omega|\psi(t)| + \mathcal{W}_\Omega) + \frac{ab}{AB(a)\Gamma(a)} \times (Q_\Omega|\psi(t)| + \mathcal{W}_\Omega)t_2^{a+b-1}\mathcal{M}(a,b) \\
&\quad - \frac{bt_1^{b-1}(1-a)}{AB(a)}(Q_\Omega|\psi(t)| + \mathcal{W}_\Omega) - \frac{ab}{AB(a)\Gamma(a)} \times (Q_\Omega|\psi(t)| + \mathcal{W}_\Omega)t_1^{a+b-1}\mathcal{M}(a,b),
\end{aligned}$$

when $t_1 \to t_2$ then $|\Pi(\psi)(t_2) - \Pi(\psi)(t_1)| \to 0$. Consequently, we can say that $\|\Pi(\psi)(t_2) - \Pi(\psi)(t_1)\| \to 0$, as $t_1 \to t_2$.

Consequently, Π is equi-continuous. Thus, by the Arzelá–Ascoli theorem, it is completely continuous. Therefore, according to fixed-point Schauder's theorem, the suggested framework possesses at least a singular solution. □

Theorem 3.5. *Presume that* (18) *applies. If* $\varrho < 1$, *where*

$$\varrho = \left(\frac{bt_2^{b-1}(1-a)}{AB(a)} + \frac{ab}{AB(a)\Gamma(a)}t^{a+b-1}\mathcal{M}(a,b)\right)\mathcal{P}_\Omega.$$

Hence, the model question has a unique solution.

Proof. For any $\psi, \overline{\psi} \in \mathcal{C}$, we obtain

$$\begin{aligned}
&|\Pi(\psi) - \Pi(\overline{\psi})| \\
&= \max_{t\in[0,\tau]} \left|\frac{bt^{b-1}(1-a)}{AB(a)}(\Omega(t,\psi(t)) - \Omega(t,\overline{\psi}(t))) + \frac{ab}{AB(a)\Gamma(a)}\int_0^t \sigma^{b-1}(t-\sigma)^{b-1}d\sigma\right.
\end{aligned}$$

$$\times(\Omega(\sigma,\psi(\sigma))-\Omega(\sigma,\overline{\psi}(\sigma)))\Big|$$

$$\leq\left[\frac{bt^{b-1}(1-a)}{AB(a)}+\frac{ab}{AB(a)\Gamma(a)}t^{a+b-1}\mathcal{M}(a,b)\right]\times\|\psi-\overline{\psi}\|$$

$$\leq\varrho\|\psi-\overline{\psi}\|.$$

Thus, Π functions as a contraction. Therefore, by the Banach contraction theorem, the proposed model has a unique solution. □

3.10. UH Stability

In this section, we analyzed the UH stability of the proposed system.

Definition 4. The suggested system will be UH stable if $\exists\ \mathfrak{K}_{\mathfrak{a},\mathfrak{b}}\geq 0$ such that for every $\varepsilon>0$ and for each $\psi\in(\mathcal{M}[0,\tau],\Re)$ verifying the subsequent inequality.

$$|{}^{\mathrm{FFM}}_{0}\mathcal{D}^{a,b}_{0}\psi(t)-(\Omega(t,\psi(t))|\leq\varepsilon, t\in[0,\tau]$$

and there is a solitary solution

$$\Theta\in(\mathcal{M}[0,\tau],\Re),$$

such that

$$|\psi(t)-\Theta(t)|\leq\mathcal{N}_{a,b}\varepsilon, t\in[0,\tau].$$

Take into account a slight disturbance $\phi\in[0,\tau]$ so that $\phi(0)=0$. Allow

- $|\phi(t)|\leq\varepsilon$ for $\varepsilon>0$.
- ${}^{\mathrm{FFM}}_{0}\mathcal{D}^{a,b}_{0}\psi(t)=(\Omega(t,\psi(t))+\phi(t)$.

Lemma 5. *The outcome of the modified system*

$${}^{\mathrm{FFM}}_{0}\mathcal{D}^{a,b}_{0}\psi(t)=(\Omega(t,\psi(t))+\phi(t)$$
$$\psi(0)=\psi_0,$$

meets the correlation outlined below.

$$\left|\mathcal{N}(t)-\left(\psi(0)+\frac{bt^{b-1}(1-a)}{AB(a)}\Omega(t,\psi(t))+\frac{ab}{AB(a)\Gamma(a)}\times\int_0^t\sigma^{b-1}(t-\sigma)^{b-1}\Omega(\sigma,\psi(\sigma))d\sigma\right)\right|\leq a^*_{a,b}\varepsilon, \tag{19}$$

$$a^*_{a,b}=\frac{bT^{b-1}(1-a)}{AB(a)}+\frac{ab}{AB(a)\Gamma(a)}T^{a+b-1}\mathcal{M}(a,b).$$

Proof. The proof is straightforward. By considering (16), one can demonstrate. By manipulating the left-hand side of (19), the desired results can be obtained. □

Lemma 6. *Subject to condition* (18) *in conjunction alongside Lemma* 5*, the resolution of the suggested framework exhibits UH stable if* $\varrho<1$.

Proof. Allow $\Theta\in\mathcal{B}$ be a singular outcome and $\psi\in\mathcal{B}$ be any outcome of the system, therefore

$$\begin{aligned}
&|\psi(t)-\Theta(t)|\\
&=\left|\psi(t)-\left(\Theta(0)+\frac{bt^{b-1}(1-a)}{AB(a)}\Omega(t,\Theta(t))+\frac{ab}{AB(a)\Gamma(a)}\int_0^t\sigma^{b-1}(t-\sigma)^{b-1}\Omega(\sigma,\Theta(\sigma))d\sigma\right)\right|\\
&\leq\left|\psi(t)-\left(\psi(0)+\frac{bt^{b-1}(1-a)}{AB(a)}\Omega(t,\psi(t))+\frac{ab}{AB(a)\Gamma(a)}\int_0^t\sigma^{b-1}(t-\sigma)^{b-1}\Omega(\sigma,\psi(\sigma))d\sigma\right)\right|\\
&\quad\dot{+}\left|\psi(0)+\frac{bt^{b-1}(1-a)}{AB(a)}\Omega(t,\psi(t))+\frac{ab}{AB(a)\Gamma(a)}\times\int_0^t\sigma^{b-1}(t-\sigma)^{b-1}\Omega(\sigma,\psi(\sigma))d\sigma\right|\\
&\quad-\left|\Theta(0)+\frac{bt^{b-1}(1-a)}{AB(a)}\Omega(t,\Theta(t))+\frac{ab}{AB(a)\Gamma(a)}\times\int_0^t\sigma^{b-1}(t-\sigma)^{b-1}\Omega(\sigma,\Theta(\sigma))d\sigma\right|\\
&\leq a^*_{a,b}\varepsilon+\left(\frac{bt^{b-1}(1-a)}{AB(a)}+\frac{ab}{AB(a)\Gamma(a)}t^{a+b-1}\mathcal{M}(a,b)\right)\times P_{\Pi}|\psi(t)-\Theta(t)|\\
&\leq a^*_{a,b}\varepsilon+\varrho|\psi(t)-\Theta(t)|.
\end{aligned}$$

Consequently, it can be written as

$$\|\psi-\Theta\|\leq a^*_{a,b}\varepsilon+\varrho\|\psi-\Theta\|.$$

The relation mentioned earlier can be expressed as

$$\|\psi-\Theta\|\leq\mathcal{N}_{a,b}\varepsilon,$$

where

$$\mathcal{N}_{a,b}=\frac{a^*_{a,b}}{1-\varrho}.$$

Thus, the system's outcome shows UH stability. □

4. NUMERICAL ANALYSIS

In this section, we derive the computational scheme for the proposed system by employing the Atangana–Baleanu fractional operators in conjunction with a Lagrangian piecewise approximation. The methodology is based on the Adams–Bashforth technique, which ensures numerical accuracy and stability. By extending the mathematical model presented below, within the framework of the Caputo sense and incorporating the Atangana–Baleanu perspective for fractional integrals, we obtain:

$$\begin{cases}
\mathcal{S}(t) = \mathcal{S}(0) + \dfrac{bt^{b-1}(1-a)}{AB(a)}\boldsymbol{Z}_1(t,\mathcal{S},\mathcal{E},\mathcal{V},\mathcal{I},\mathcal{H},\mathcal{R}) + \dfrac{ab}{AB(a)\Gamma(a)}\displaystyle\int_0^t \sigma^{b-1}(t-\sigma)\boldsymbol{Z}_1(\sigma,\mathcal{S},\mathcal{E},\mathcal{V},\mathcal{I},\mathcal{H},\mathcal{R})d\sigma,\\
\mathcal{E}(t) = \mathcal{E}(0) + \dfrac{bt^{b-1}(1-a)}{AB(a)}\boldsymbol{Z}_2(t,\mathcal{S},\mathcal{E},\mathcal{V},\mathcal{I},\mathcal{H},\mathcal{R}) + \dfrac{ab}{AB(a)\Gamma(a)}\displaystyle\int_0^t \sigma^{b-1}(t-\sigma)\boldsymbol{Z}_2(\sigma,\mathcal{S},\mathcal{E},\mathcal{V},\mathcal{I},\mathcal{H},\mathcal{R})d\sigma,\\
\mathcal{V}(t) = \mathcal{V}(0) + \dfrac{bt^{b-1}(1-a)}{AB(a)}\boldsymbol{Z}_3(t,\mathcal{S},\mathcal{E},\mathcal{V},\mathcal{I},\mathcal{H},\mathcal{R}) + \dfrac{ab}{AB(a)\Gamma(a)}\displaystyle\int_0^t \sigma^{b-1}(t-\sigma)\boldsymbol{Z}_3(\sigma,\mathcal{S},\mathcal{E},\mathcal{V},\mathcal{I},\mathcal{H},\mathcal{R})d\sigma,\\
\mathcal{I}(t) = \mathcal{I}(0) + \dfrac{bt^{b-1}(1-a)}{AB(a)}\boldsymbol{Z}_4(t,\mathcal{S},\mathcal{E},\mathcal{V},\mathcal{I},\mathcal{H},\mathcal{R}) + \dfrac{ab}{AB(a)\Gamma(a)}\displaystyle\int_0^t \sigma^{b-1}(t-\sigma)\boldsymbol{Z}_4(\sigma,\mathcal{S},\mathcal{E},\mathcal{V},\mathcal{I},\mathcal{H},\mathcal{R})d\sigma,\\
\mathcal{H}(t) = \mathcal{H}(0) + \dfrac{bt^{b-1}(1-a)}{AB(a)}\boldsymbol{Z}_5(t,\mathcal{S},\mathcal{E},\mathcal{V},\mathcal{I},\mathcal{H},\mathcal{R}) + \dfrac{ab}{AB(a)\Gamma(a)}\displaystyle\int_0^t \sigma^{b-1}(t-\sigma)\boldsymbol{Z}_5(\sigma,\mathcal{S},\mathcal{E},\mathcal{V},\mathcal{I},\mathcal{H},\mathcal{R})d\sigma,\\
\mathcal{R}(t) = \mathcal{R}(0) + \dfrac{bt^{b-1}(1-a)}{AB(a)}\boldsymbol{Z}_6(t,\mathcal{S},\mathcal{E},\mathcal{V},\mathcal{I},\mathcal{H},\mathcal{R}) + \dfrac{ab}{AB(a)\Gamma(a)}\displaystyle\int_0^t \sigma^{b-1}(t-\sigma)\boldsymbol{Z}_6(\sigma,\mathcal{S},\mathcal{E},\mathcal{V},\mathcal{I},\mathcal{H},\mathcal{R})d\sigma.
\end{cases} \tag{20}$$

The system of equations described in (20) characterizes the dynamics of a fractional-order model involving multiple compartments: $\mathcal{S}(t)$ (susceptible), $\mathcal{E}(t)$ (exposed), $\mathcal{V}(t)$ (vaccinated), $\mathcal{I}(t)$ (infected), $\mathcal{H}(t)$ (hospitalized), and $\mathcal{R}(t)$ (recovered). The model leverages the Atangana–Baleanu fractional derivative, which is particularly effective in describing complex systems with memory-dependent processes, such as those encountered in epidemiological modeling. Next, we derive the numerical scheme at $t = t_{n+1}$, We have

$$\begin{cases}
\mathcal{S}^{n+1} = \mathcal{S}^0 + \dfrac{bt^{b-1}(1-a)}{AB(a)}\boldsymbol{Z}_1(t_n,\mathcal{S}^n,\mathcal{E}^n,\mathcal{V}^n,\mathcal{I}^n,\mathcal{H}^n,\mathcal{R}^n)\\
\qquad + \dfrac{ab}{AB(a)\Gamma(a)}\displaystyle\int_0^t \sigma^{b-1}(t-\sigma)^{b-1}\boldsymbol{Z}_1(\sigma,\mathcal{S},\mathcal{E},\mathcal{V},\mathcal{I},\mathcal{H},\mathcal{R})d\sigma,\\
\mathcal{E}^{n+1} = \mathcal{E}^0 + \dfrac{bt^{b-1}(1-a)}{AB(a)}\boldsymbol{Z}_2(t_n,\mathcal{S}^n,\mathcal{E}^n,\mathcal{V}^n,\mathcal{I}^n,\mathcal{H}^n,\mathcal{R}^n)\\
\qquad + \dfrac{ab}{AB(a)\Gamma(a)}\displaystyle\int_0^t \sigma^{b-1}(t-\sigma)^{b-1}\boldsymbol{Z}_2(\sigma,\mathcal{S},\mathcal{E},\mathcal{V},\mathcal{I},\mathcal{H},\mathcal{R})d\sigma,\\
\mathcal{V}^{n+1} = \mathcal{V}^0 + \dfrac{bt^{b-1}(1-a)}{AB(a)}\boldsymbol{Z}_3(t_n,\mathcal{S}^n,\mathcal{E}^n,\mathcal{V}^n,\mathcal{I}^n,\mathcal{H}^n,\mathcal{R}^n)\\
\qquad + \dfrac{ab}{AB(a)\Gamma(a)}\displaystyle\int_0^t \sigma^{b-1}(t-\sigma)^{b-1}\boldsymbol{Z}_3(\sigma,\mathcal{S},\mathcal{E},\mathcal{V},\mathcal{I},\mathcal{H},\mathcal{R})d\sigma,
\end{cases}$$

$$\begin{cases} \mathcal{I}^{n+1} = \mathcal{I}^0 + \dfrac{bt^{b-1}(1-a)}{AB(a)}\boldsymbol{Z}_4(t_n, \mathcal{S}^n, \mathcal{E}^n, \mathcal{V}^n, \mathcal{I}^n, \mathcal{H}^n, \mathcal{R}^n) \\ \qquad + \dfrac{ab}{AB(a)\Gamma(a)}\displaystyle\int_0^t \sigma^{b-1}(t-\sigma)^{b-1}\boldsymbol{Z}_4(\sigma, \mathcal{S}, \mathcal{E}, \mathcal{V}, \mathcal{I}, \mathcal{H}, \mathcal{R})d\sigma, \\ \mathcal{H}^{n+1} = \mathcal{H}^0 + \dfrac{bt^{b-1}(1-a)}{AB(a)}\boldsymbol{Z}_5(t_n, \mathcal{S}^n, \mathcal{E}^n, \mathcal{V}^n, \mathcal{I}^n, \mathcal{H}^n, \mathcal{R}^n) \\ \qquad + \dfrac{ab}{AB(a)\Gamma(a)}\displaystyle\int_0^t \sigma^{b-1}(t-\sigma)^{b-1}\boldsymbol{Z}_5(\sigma, \mathcal{S}, \mathcal{E}, \mathcal{V}, \mathcal{I}, \mathcal{H}, \mathcal{R})d\sigma, \\ \mathcal{R}^{n+1} = \mathcal{R}^0 + \dfrac{bt^{b-1}(1-a)}{AB(a)}\boldsymbol{Z}_6(t_n, \mathcal{S}^n, \mathcal{E}^n, \mathcal{V}^n, \mathcal{I}^n, \mathcal{H}^n, \mathcal{R}^n) \\ \qquad + \dfrac{ab}{AB(a)\Gamma(a)}\displaystyle\int_0^t \sigma^{b-1}(t-\sigma)^{b-1}\boldsymbol{Z}_6(\sigma, \mathcal{S}, \mathcal{E}, \mathcal{V}, \mathcal{I}, \mathcal{H}, \mathcal{R})d\sigma. \end{cases} \tag{21}$$

The system in (21) represents the numerical iteration for the fractional-order model, incorporating the memory effects of past states. Each compartment $\mathcal{X}^{n+1}$ (e.g. $\mathcal{S}$, $\mathcal{E}$, $\mathcal{V}$, $\mathcal{I}$, $\mathcal{H}$, $\mathcal{R}$) at step $n+1$ is determined by $\mathcal{X}^0$, the initial state of each compartment.

$$\frac{bt^{b-1}(1-a)}{AB(a)}\boldsymbol{Z}_i(t_n, \mathcal{S}^n, \mathcal{E}^n, \mathcal{V}^n, \mathcal{I}^n, \mathcal{H}^n, \mathcal{R}^n),$$

capturing instantaneous dynamics based on the current states.

$$\frac{ab}{AB(a)\Gamma(a)}\int_0^t \sigma^{b-1}(t-\sigma)^{b-1}\boldsymbol{Z}_i(\sigma, \mathcal{S}, \mathcal{E}, \mathcal{V}, \mathcal{I}, \mathcal{H}, \mathcal{R})\, d\sigma,$$

representing the cumulative effects of past interactions weighted by the fractional kernel.

By approximating the integral on the right-hand side of the system (21), we obtain

$$\begin{cases} \mathcal{S}^{n+1} = \mathcal{S}^0 + \dfrac{bt_n^{b-1}(1-a)}{AB(a)}\boldsymbol{Z}_1(t_n, \mathcal{S}^n, \mathcal{E}^n, \mathcal{V}^n, \mathcal{I}^n, \mathcal{H}^n, \mathcal{R}^n) \\ \qquad + \dfrac{ab}{AB(a)\Gamma(a)}\displaystyle\sum_{m=0}^{n}\int_{t_m}^{t_{m+1}} \sigma^{b-1}(t_{n+1}-\sigma)^{b-1}\boldsymbol{Z}_1(\sigma, \mathcal{S}, \mathcal{E}, \mathcal{V}, \mathcal{I}, \mathcal{H}, \mathcal{R})d\sigma, \\ \mathcal{E}^{n+1} = \mathcal{E}^0 + \dfrac{bt_n^{b-1}(1-a)}{AB(a)}\boldsymbol{Z}_2(t_n, \mathcal{S}^n, \mathcal{E}^n, \mathcal{V}^n, \mathcal{I}^n, \mathcal{H}^n, \mathcal{R}^n) \\ \qquad + \dfrac{ab}{AB(a)\Gamma(a)}\displaystyle\sum_{m=0}^{n}\int_{t_m}^{t_{m+1}} \sigma^{b-1}(t_{n+1}-\sigma)^{b-1}\boldsymbol{Z}_2(\sigma, \mathcal{S}, \mathcal{E}, \mathcal{V}, \mathcal{I}, \mathcal{H}, \mathcal{R})d\sigma, \\ \mathcal{V}^{n+1} = \mathcal{V}^0 + \dfrac{bt_n^{b-1}(1-a)}{AB(a)}\boldsymbol{K}_3(t_n, \mathcal{S}^n, \mathcal{E}^n, \mathcal{V}^n, \mathcal{I}^n, \mathcal{H}^n, \mathcal{R}^n) \\ \qquad + \dfrac{ab}{AB(a)\Gamma(a)}\displaystyle\sum_{m=0}^{n}\int_{t_m}^{t_{m+1}} \sigma^{b-1}(t_{n+1}-\sigma)^{b-1}\boldsymbol{Z}_3(\sigma, \mathcal{S}, \mathcal{E}, \mathcal{V}, \mathcal{I}, \mathcal{H}, \mathcal{R})d\sigma, \end{cases}$$

$$
\begin{cases}
\mathcal{I}^{n+1} = \mathcal{I}^0 + \dfrac{bt_n^{b-1}(1-a)}{AB(a)}\boldsymbol{Z}_4(t_n, \mathcal{S}^n, \mathcal{E}^n, \mathcal{V}^n, \mathcal{I}^n, \mathcal{H}^n, \mathcal{R}^n) \\
\qquad + \dfrac{ab}{AB(a)\Gamma(a)}\displaystyle\sum_{m=0}^{n}\int_{t_m}^{t_{m+1}} \sigma^{b-1}(t_{n+1}-\sigma)^{b-1}\boldsymbol{Z}_4(\sigma, \mathcal{S}, \mathcal{E}, \mathcal{V}, \mathcal{I}, \mathcal{H}, \mathcal{R})d\sigma, \\
\mathrm{H}^{n+1} = \mathcal{H}^0 + \dfrac{bt_n^{b-1}(1-a)}{AB(a)}\boldsymbol{Z}_5(t_n, \mathcal{S}^n, \mathcal{E}^n, \mathcal{V}^n, \mathcal{I}^n, \mathcal{H}^n, \mathcal{R}^n) \\
\qquad + \dfrac{ab}{AB(a)\Gamma(a)}\displaystyle\sum_{m=0}^{n}\int_{t_m}^{t_{m+1}} \sigma^{b-1}(t_{n+1}-\sigma)^{b-1}\boldsymbol{Z}_5(\sigma, \mathcal{S}, \mathcal{E}, \mathcal{V}, \mathcal{I}, \mathcal{H}, \mathcal{R})d\sigma, \\
\mathrm{R}^{n+1} = \mathcal{R}^0 + \dfrac{bt_n^{b-1}(1-a)}{AB(a)}\boldsymbol{Z}_6(t_n, \mathcal{S}^n, \mathcal{E}^n, \mathcal{V}^n, \mathcal{I}^n, \mathcal{H}^n, \mathcal{R}^n) \\
\qquad + \dfrac{ab}{AB(a)\Gamma(a)}\displaystyle\sum_{m=0}^{n}\int_{t_m}^{t_{m+1}} \sigma^{b-1}(t_{n+1}-\sigma)^{b-1}\boldsymbol{Z}_6(\sigma, \mathcal{S}, \mathcal{E}, \mathcal{V}, \mathcal{I}, \mathcal{H}, \mathcal{R})d\sigma.
\end{cases} \tag{22}
$$

The system in (22) describes a system of fractional-order difference equations for six variables $\mathcal{S}$, $\mathcal{E}$, $\mathcal{V}$, $\mathcal{I}$, $\mathcal{H}$, and $\mathcal{R}$, evolving stepwise (n). This system models processes incorporating memory or fractional dynamics, such as epidemiology or fluid flow.

We estimate the kernel within the essential by employing Lagrangian piecewise interpolation within the finite interval $[t_m, t_{m+1}]$ as follows:

$$
\begin{cases}
A_m(\sigma) = \dfrac{\sigma - t_{m-1}}{t_m - t_{m-1}}t_m^b\boldsymbol{Z}_1(t, \mathcal{S}, \mathcal{E}, \mathcal{V}, \mathcal{I}, \mathcal{H}, \mathcal{R}) - \dfrac{\sigma - t_m}{t_m - t_{m-1}}t_{m-1}^{b-1} \\
\qquad \times \boldsymbol{Z}_1(t_n, \mathcal{S}^{m-1}, \mathcal{E}^{m-1}, \mathcal{V}^{m-1}, \mathcal{I}^{m-1}, \mathcal{H}^{m-1}, \mathcal{R}^{m-1}), \\
B_m(\sigma) = \dfrac{\sigma - t_{m-1}}{t_m - t_{m-1}}t_m^b\boldsymbol{Z}_2(t, \mathcal{S}, \mathcal{E}, \mathcal{V}, \mathcal{I}, \mathcal{H}, \mathcal{R}) - \dfrac{\sigma - t_m}{t_m - t_{m-1}}t_{m-1}^{b-1} \\
\qquad \times \boldsymbol{Z}_2(t_n, \mathcal{S}^{m-1}, \mathcal{E}^{m-1}, \mathcal{V}^{m-1}, \mathcal{I}^{m-1}, \mathcal{H}^{m-1}, \mathcal{R}^{m-1}), \\
C_m(\sigma) = \dfrac{\sigma - t_{m-1}}{t_m - t_{m-1}}t_m^b\boldsymbol{Z}_3(t, \mathcal{S}, \mathcal{E}, \mathcal{V}, \mathcal{I}, \mathcal{H}, \mathcal{R}) - \dfrac{\sigma - t_m}{t_m - t_{m-1}}t_{m-1}^{b-1} \\
\qquad \times \boldsymbol{Z}_3(t_n, \mathcal{S}^{m-1}, \mathcal{E}^{m-1}, \mathcal{V}^{m-1}, \mathcal{I}^{m-1}, \mathcal{H}^{m-1}, \mathcal{R}^{m-1}), \\
D_m(\sigma) = \dfrac{\sigma - t_{m-1}}{t_m - t_{m-1}}t_m^b\boldsymbol{Z}_4(t, \mathcal{S}, \mathcal{E}, \mathcal{V}, \mathcal{I}, \mathcal{H}, \mathcal{R}) - \dfrac{\sigma - t_m}{t_m - t_{m-1}}t_{m-1}^{b-1} \\
\qquad \times \boldsymbol{Z}_4(t_n, \mathcal{S}^{m-1}, \mathcal{E}^{m-1}, \mathcal{V}^{m-1}, \mathcal{I}^{m-1}, \mathcal{H}^{m-1}, \mathcal{R}^{m-1}), \\
E_m(\sigma) = \dfrac{\sigma - t_{m-1}}{t_m - t_{m-1}}t_m^b\boldsymbol{Z}_5(t, \mathcal{S}, \mathcal{E}, \mathcal{V}, \mathcal{I}, \mathcal{H}, \mathcal{R}) - \dfrac{\sigma - t_m}{t_m - t_{m-1}}t_{m-1}^{b-1} \\
\qquad \times \boldsymbol{Z}_5(t_n, \mathcal{S}^{m-1}, \mathcal{E}^{m-1}, \mathcal{V}^{m-1}, \mathcal{I}^{m-1}, \mathcal{H}^{m-1}, \mathcal{R}^{m-1}), \\
F_m(\sigma) = \dfrac{\sigma - t_{m-1}}{t_m - t_{m-1}}t_m^b\boldsymbol{Z}_6(t, \mathcal{S}, \mathcal{E}, \mathcal{V}, \mathcal{I}, \mathcal{H}, \mathcal{R}) - \dfrac{\sigma - t_m}{t_m - t_{m-1}}t_{m-1}^{b-1} \\
\qquad \times \boldsymbol{Z}_6(t_n, \mathcal{S}^{m-1}, \mathcal{E}^{m-1}, \mathcal{V}^{m-1}, \mathcal{I}^{m-1}, \mathcal{H}^{m-1}, \mathcal{R}^{m-1}).
\end{cases}
$$

Utilizing Lagrangian polynomial piecewise interpolation, we obtain

$$
\begin{cases}
\mathcal{S}^{n+1} = \mathcal{S}^0 + \dfrac{bt_n^{b-1}(1-a)}{AB(a)}\boldsymbol{Z}_1(t_n,\mathcal{S}^n,\mathcal{E}^n,\mathcal{V}^n,\mathcal{I}^n,\mathcal{H}^n,\mathcal{R}^n) + \dfrac{ab}{AB(a)\Gamma(a)}, \\
\quad \displaystyle\sum_{m=0}^{n} \begin{bmatrix} t_n^{b-1}\boldsymbol{Z}_1(t_n,\mathcal{S}^n,\mathcal{E}^n,\mathcal{V}^n,\mathcal{I}^n,\mathcal{H}^n,\mathcal{R}^n)((n+1-m)^a(n-m+2+a) \\ \quad -(n-m)^a(2+2a+n-m)), \\ -t_{n-1}^{b-1}\boldsymbol{Z}_1(t_{n-1},\mathcal{S}^{n-1},\mathcal{E}^{n-1},\mathcal{V}^{n-1},\mathcal{I}^{n-1},\mathcal{H}^{n-1},\mathcal{R}^{n-1})((1+n-m)^{a+1} \\ \quad -(n-m)^a(1+a+n-m)), \end{bmatrix}, \\
\mathcal{E}^{n+1} = \mathcal{E}^0 + \dfrac{bt_n^{b-1}(1-a)}{AB(a)}\boldsymbol{Z}_2(t_n,\mathcal{S}^n,\mathcal{E}^n,\mathcal{V}^n,\mathcal{I}^n,\mathcal{H}^n,\mathcal{R}^n) + \dfrac{ab}{AB(a)\Gamma(a)}, \\
\quad \displaystyle\sum_{m=0}^{n} \begin{bmatrix} t_n^{b-1}\boldsymbol{Z}_2(t_n,\mathcal{S}^n,\mathcal{E}^n,\mathcal{V}^n,\mathcal{I}^n,\mathcal{H}^n,\mathcal{R}^n)((n+1-m)^a(n-m+2+a) \\ \quad -(n-m)^a(2+2a+n-m)), \\ -t_{n-1}^{b-1}\boldsymbol{Z}_2(t_{n-1},\mathcal{S}^{n-1},\mathcal{E}^{n-1},\mathcal{V}^{n-1},\mathcal{I}^{n-1},\mathcal{H}^{n-1},\mathcal{R}^{n-1})((1+n-m)^{a+1} \\ \quad -(n-m)^a(1+a+n-m)), \end{bmatrix}, \\
\mathcal{V}^{n+1} = \mathcal{V}^0 + \dfrac{bt_n^{b-1}(1-a)}{AB(a)}\boldsymbol{2}_3(t_n,\mathcal{S}^n,\mathcal{E}^n,\mathcal{V}^n,\mathcal{I}^n,\mathcal{H}^n,\mathcal{R}^n) + \dfrac{ab}{AB(a)\Gamma(a)}, \\
\quad \displaystyle\sum_{m=0}^{n} \begin{bmatrix} t_n^{b-1}\boldsymbol{Z}_3(t_n,\mathcal{S}^n,\mathcal{E}^n,\mathcal{V}^n,\mathcal{I}^n,\mathcal{H}^n,\mathcal{R}^n)((n+1-m)^a(n-m+2+a) \\ \quad -(n-m)^a(2+2a+n-m)) \\ -t_{n-1}^{b-1}\boldsymbol{Z}_3(t_{n-1},\mathcal{S}^{n-1},\mathcal{E}^{n-1},\mathcal{V}^{n-1},\mathcal{I}^{n-1},\mathcal{H}^{n-1},\mathcal{R}^{n-1})((1+n-m)^{a+1} \\ \quad -(n-m)^a(1+a+n-m)) \end{bmatrix}, \\
\mathcal{I}^{n+1} = \mathcal{I}^0 + \dfrac{bt_n^{b-1}(1-a)}{AB(a)}\boldsymbol{Z}_4(t_n,\mathcal{S}^n,\mathcal{E}^n,\mathcal{V}^n,\mathcal{I}^n,\mathcal{H}^n,\mathcal{R}^n) + \dfrac{ab}{AB(a)\Gamma(a)}, \\
\quad \displaystyle\sum_{m=0}^{n} \begin{bmatrix} t_n^{b-1}\boldsymbol{Z}_4(t_n,\mathcal{S}^n,\mathcal{E}^n,\mathcal{V}^n,\mathcal{I}^n,\mathcal{H}^n,\mathcal{R}^n)((n+1-m)^a(n-m+2+a) \\ \quad -(n-m)^a(2+2a+n-m)) \\ -t_{n-1}^{b-1}\boldsymbol{Z}_4(t_{n-1},\mathcal{S}^{n-1},\mathcal{E}^{n-1},\mathcal{V}^{n-1},\mathcal{I}^{n-1},\mathcal{H}^{n-1},\mathcal{R}^{n-1})((1+n-m)^{a+1} \\ \quad -(n-m)^a(1+a+n-m)) \end{bmatrix}, \\
\mathcal{H}^{n+1} = \mathcal{H}^0 + \dfrac{bt_n^{b-1}(1-a)}{AB(a)}\boldsymbol{Z}_5(t_n,\mathcal{S}^n,\mathcal{E}^n,\mathcal{V}^n,\mathcal{I}^n,\mathcal{H}^n,\mathcal{R}^n) + \dfrac{ab}{AB(a)\Gamma(a)}, \\
\quad \displaystyle\sum_{m=0}^{n} \begin{bmatrix} t_n^{b-1}\boldsymbol{Z}_5(t_n,\mathcal{S}^n,\mathcal{E}^n,\mathcal{V}^n,\mathcal{I}^n,\mathcal{H}^n,\mathcal{R}^n)((n+1-m)^a(n-m+2+a) \\ \quad -(n-m)^a(2+2a+n-m)) \\ -t_{n-1}^{b-1}\boldsymbol{Z}_5(t_{n-1},\mathcal{S}^{n-1},\mathcal{E}^{n-1},\mathcal{V}^{n-1},\mathcal{I}^{n-1},\mathcal{H}^{n-1},\mathcal{R}^{n-1})((1+n-m)^{a+1} \\ \quad -(n-m)^a(1+a+n-m)) \end{bmatrix}, \\
\mathcal{R}^{n+1} = \mathcal{R}^0 + \dfrac{bt_n^{b-1}(1-a)}{AB(a)}\boldsymbol{Z}_5(t_n,\mathcal{S}^n,\mathcal{E}^n,\mathcal{V}^n,\mathcal{I}^n,\mathcal{H}^n,\mathcal{R}^n) + \dfrac{ab}{AB(a)\Gamma(a)}, \\
\quad \displaystyle\sum_{m=0}^{n} \begin{bmatrix} t_n^{b-1}\boldsymbol{Z}_6(t_n,\mathcal{S}^n,\mathcal{E}^n,\mathcal{V}^n,\mathcal{I}^n,\mathcal{H}^n,\mathcal{R}^n)((n+1-m)^a(n-m+2+a) \\ \quad -(n-m)^a(2+2a+n-m)) \\ -t_{n-1}^{b-1}\boldsymbol{Z}_6(t_{n-1},\mathcal{S}^{n-1},\mathcal{E}^{n-1},\mathcal{V}^{n-1},\mathcal{I}^{n-1},\mathcal{H}^{n-1},\mathcal{R}^{n-1})((1+n-m)^{a+1} \\ \quad -(n-m)^a(1+a+n-m)) \end{bmatrix}.
\end{cases} \tag{23}
$$

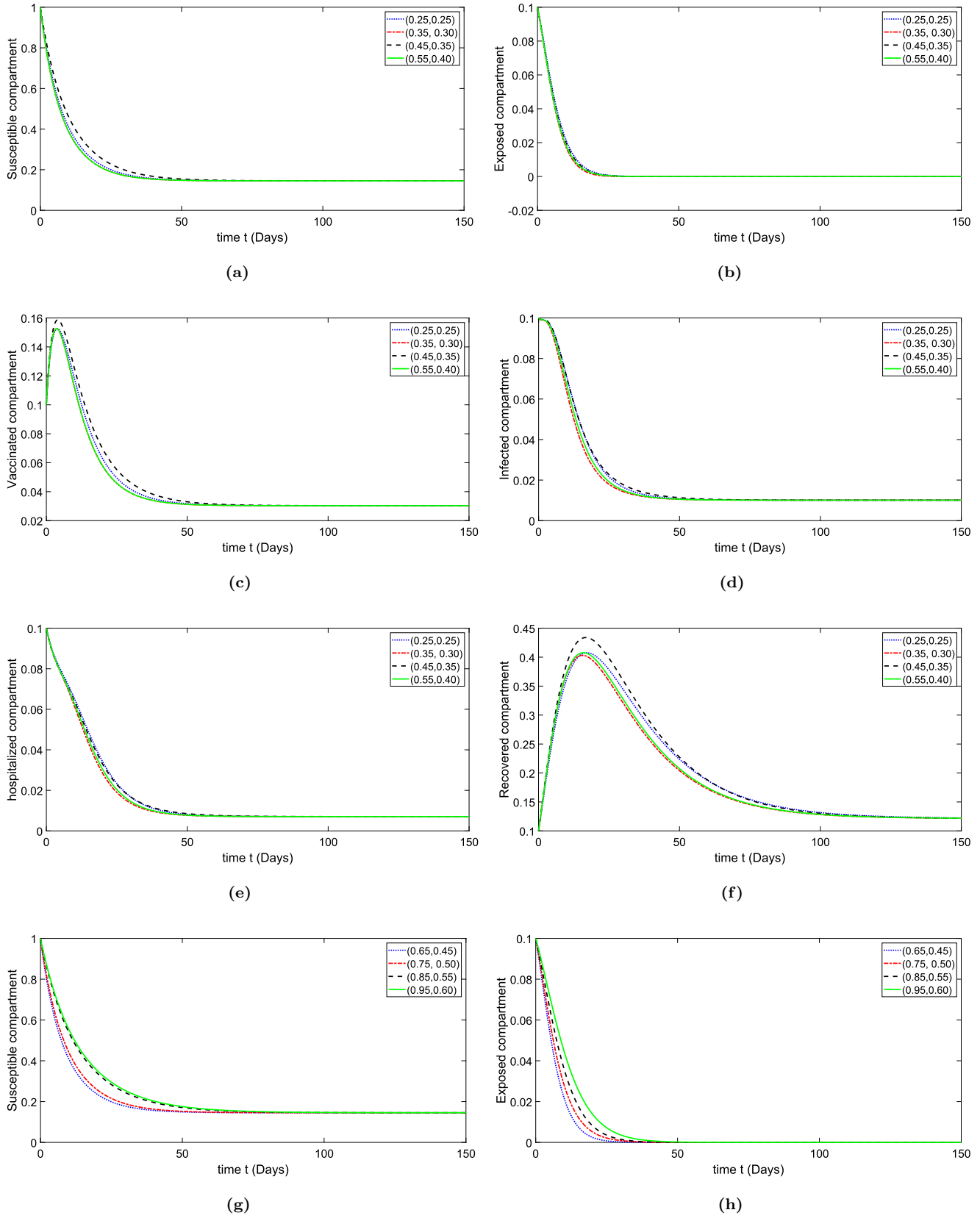

Fig. 6 Graphical representation of the approximate solutions for the compartments of the model (5) under various fractal fractional orders: **(a)** Susceptible compartment, **(b)** Exposed compartment, **(c)** Vaccinated compartment, **(d)** Infected compartment, **(e)** Hospitalized compartment, **(f)** Recovered compartment, **(g)** Susceptible compartment (repeated for verification), and **(h)** Exposed compartment (repeated for verification).

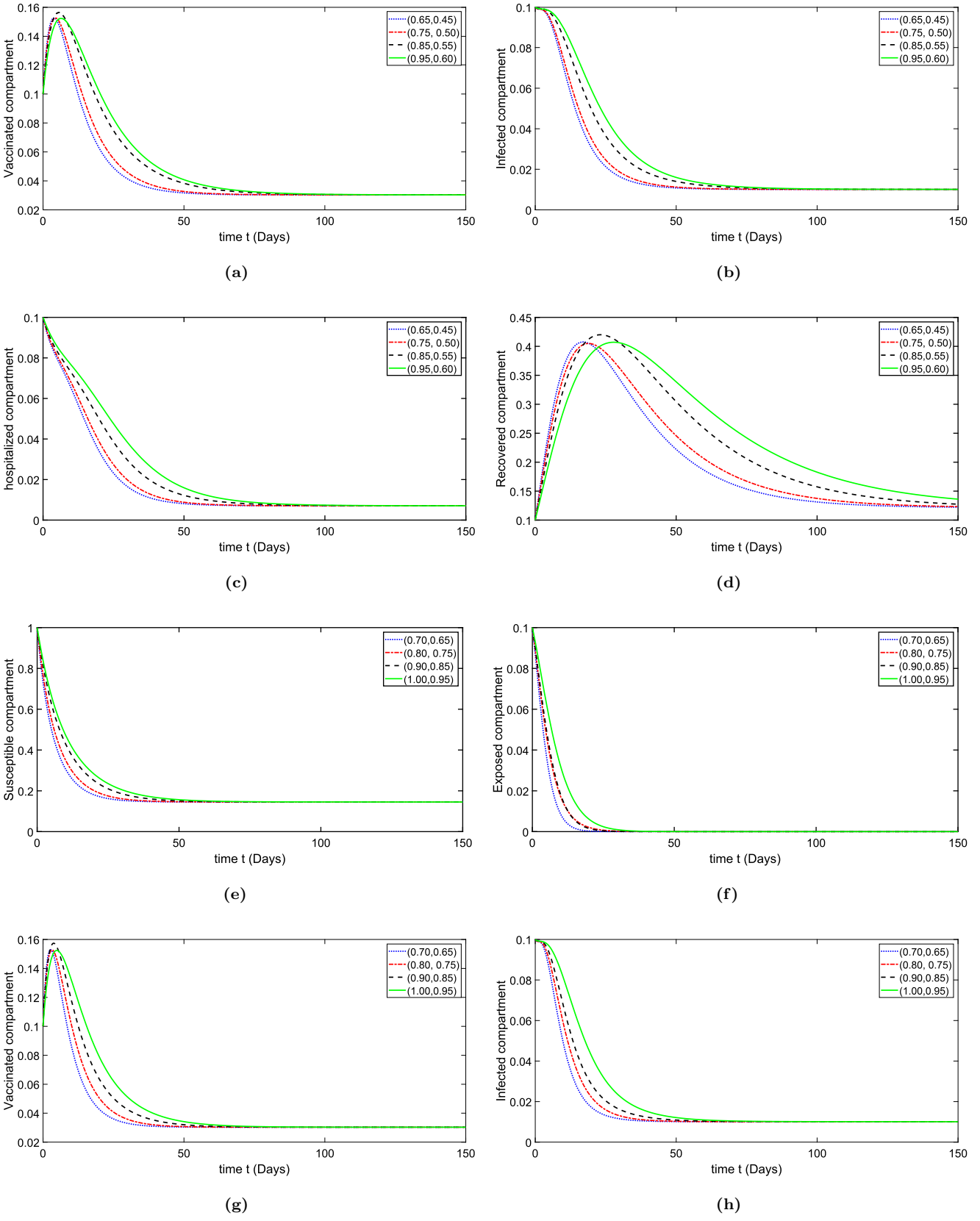

Fig. 7 Graphical representation of the approximate solutions for the compartments of the model (5) under varying fractal–fractional orders: (**a**) Vaccinated compartment, (**b**) Infected compartment, (**c**) Hospitalized compartment, (**d**) Recovered compartment, (**e**) Susceptible compartment, (**f**) Exposed compartment, (**g**) Vaccinated compartment (repeated for consistency), and (**h**) Infected compartment (repeated for consistency).

The equations utilize Lagrangian polynomial interpolation to approximate the evolution of the system variables $\mathcal{S}, \mathcal{E}, \mathcal{V}, \mathcal{I}, \mathcal{H}, \mathcal{R}$ over discrete time steps. The terms $A_m(\sigma)$, $B_m(\sigma)$, $C_m(\sigma)$, $D_m(\sigma)$, $E_m(\sigma)$, and $F_m(\sigma)$ represent piecewise interpolated contributions that depend on the states at previous time points t_{m-1} and t_m. Equation (23) provides a numerical framework to capture the fractional-order dynamics, ensuring smooth transitions across time steps and effectively modeling systems with memory and long-range dependencies.

5. NUMERICAL SIMULATIONS

In this section, we present the computational results and provide a comprehensive analysis of the system's approximate solutions by employing a carefully selected numerical methodology. The parameter values utilized in the system are summarized in Table 3. A comparative analysis of various compartments of Model (5) is carried out under different fractional orders, while the fractal order values remain fixed. The numerical solutions for both classical and fractional cases, derived using the ABC fractional derivative, are illustrated in Fig. 6. These graphical representations capture the trends and findings from the analysis, highlighting the impact of varying fractional orders. It is observed that as the fractional-order decreases, the number of susceptible individuals increases, whereas other compartments, such as exposed, vaccinated, infected, hospitalized, and recovered, exhibit a decline with increasing fractional values. This behavior demonstrates the accuracy and efficiency of the ABC fractional derivative in modeling the system, meeting the study's requirements effectively. Furthermore, the results confirm the derivative's capability to account for complex, non-local dynamics within the system.

Additionally, graphical representations of the system's dynamics under different fractional orders and fractal conditions ($\gamma = 1$ and $\gamma = 0.99$) are presented in Fig. 7. These figures reveal that fractal conditions significantly influence the behaviors of the system's compartments, demonstrating their sensitivity to fractal–fractional parameters. The study further explores the dynamics of the proposed model through Fig. 8, using a range of fractal–fractional order (FFO) values chosen to emulate the characteristics of the Ebola virus. The comparative analysis of these results underscores the superiority of fractal–fractional order differential (FFOD) models over classical models in analyzing infectious disease dynamics. By incorporating fractional derivatives, FFOD models effectively capture the complexities of disease transmission, providing deeper insights into infection patterns and behaviors. The inherent geometric intricacies of the system, which are often overlooked in classical fractional calculus, are better addressed through the application of fractal–fractional calculus, offering a novel perspective on disease modeling. Notably, the simulations reveal that disease dynamics evolve differently with varying FFO values, achieving stability faster at lower fractional orders. As the fractional-order increases, the system's behavior converges toward the integer-order model. These findings highlight the proposed model's superiority and generality over classical models, providing a robust framework for understanding and predicting infectious disease dynamics.

In Fig. 6, the subfigures a–h highlight the behavior of the respective compartment using different

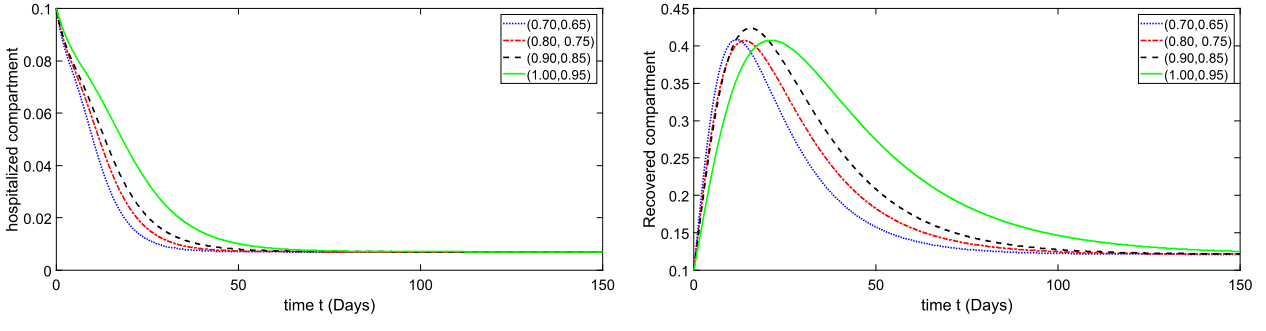

(a) **(b)**

Fig. 8 Graphical representation of the approximate solutions for the compartments of the model (5) under varying fractal–fractional orders: (**a**) Hospitalized compartment and (**b**) Recovered compartment.

fractional orders. This illustrates the sensitivity and dynamics of the model.

In Fig. 7, the subfigures a–h demonstrate the compartmental dynamics influenced by distinct fractal and fractional orders.

In Fig. 8, each subfigures a and b have highlighted the impact of different fractal and fractional orders on the dynamics of the respective compartments.

6. CONCLUSION

In this paper, we analyze a newly emerging mathematical model for the EVD. Incorporating distinct classes for vaccinated and hospitalized individuals. The primary objective the model is meant to show is the effect of hospitalization on disease control measures. We present an improved model that encompasses the ABC fractional-order derivative operators so that solutions remain non-negative. We have identified steady-state points and the basic reproductive number. In addition, we highlighted the conditions that were essentially required to perform sensitivity analysis, and discussed Banach's fixed-point theorem to establish the existence and uniqueness of solutions for the fractional system. Then, different forms are obtained from the obtained UHS and then local stability is done to confirm the nature of stability of the solution of the proposed fractional-order system. Finally, numerical schemes are developed for different fractal–fractional operators including Caputo, CF, and AB by utilizing Adams–Bashforth techniques. We have utilized MATLAB (R2019a) to inspect the results with visualization of the evolution of the Ebola virus model for the different FFOs. The results obtained from such a study are shown for six different cases, where the behavior of the model was studied for six different fractional values. Graphical representations were used to compare the fractal dimension with the variations due to the fractional order. Changes in fractal size alter the dynamics of the different compartments that comprise the system. In the numerical simulations performed, it was observed that, by changing the kernel of the FFOs, the graphical representation of the analyzed system is modified. The performed simulations also permitted establishing that fractal-fractional orders, depending on fractal dimension, can conduct to more information than the classic fractional differential coefficients. With the aim of enhancing the model, we suggest an enhancement by the inclusion of a factor that considers the causal behavior induced by significant reference points that in most instances propagate over time. This added component will lead to a model driven by the stochastic Fractional Differential Equations, the FDEs. Other proposed follow-up submissions and extensions in the current model are presented as follows:

- Comprehensive investigation of bifurcations in steady-state solutions with respect to various parameters.
- Exploration of chaotic dynamics within the system.
- Analysis of the controllability features of the proposed model.

These proposed extensions aim to enhance the predictive and analytical capabilities of the model in understanding the dynamics of the Ebola virus and similar infectious diseases.

ACKNOWLEDGMENTS

The authors extend their appreciation to the Deanship of Research and Graduate Studies at King Khalid University for funding this work through Large Research Project under Grant No. RGP2/319/46.

Authors are thankful to Prince Sultan University for APC and support through TAS research Lab.

ORCID

Ateeq Ur Rehman Irshad
https://orcid.org/0000-0001-5723-2177
Nadeem Khan
https://orcid.org/0009-0006-8970-1218
Mukhtiar Khan
https://orcid.org/0009-0003-3680-4078
Farhad Hussain
https://orcid.org/0009-0003-8578-2557
Kamal Shah
https://orcid.org/0000-0002-8851-4844
Bahaaeldin Abdalla
https://orcid.org/0000-0001-8867-0612
Khursheed J. Ansar
https://orcid.org/0000-0003-4564-6211
Thabet Abdeljawad
https://orcid.org/0000-0002-8889-3768

REFERENCES

1. E. M. Leroy, B. Kumulungui and X. Pourrut, Fruit bats as reservoirs of Ebola virus, *Nature* **438** (2015) 575–576.
2. L. Zhou and M. Fan, Dynamics of an SIR model with limited medical resources revisited, *Nonlinear Anal. Real World Appl.* **13** (2012) 312–324.
3. M. Rafiq, W. Ahmad, M. Abbas and D. Baleanu, A reliable and competitive mathematical analysis of Ebola epidemic model, *Adv. Differ. Equ.* **1** (2020) 1–24.
4. M. Asghar, M. Rafiq and M. O. Ahmad, Numerical analysis of a modified SIR epidemic model with the effect of time delay, *Punjab Univ. J. Math.* **51**(1) (2019) 79–90.
5. S. Edwarda, E. M. Lusekelob, D. M. Ndidic and E. Simanjilod, Mathematical modeling of the transmission dynamics of Ebola virus disease with control strategies, *IJSBAR* **33**(1) (2017) 112–130.
6. F. Almeida-pinto, R. Pinto and J. Rocha, Navigating the complex landscape of Ebola infection treatment: A review of emerging pharmacological approaches, *Infect. Dis. Ther.* **13**(1) (2024) 21–55.
7. B. Ivorra, D. Ngom and A. M. Ramos, Be-CoDiS: A mathematical model to predict the risk of human diseases spread between countries-validation and application to the 2014–2015 Ebola virus disease epidemic, *Bull. Math. Biol.* **77** (2015) 1668–1704.
8. W. Ahmad, M. Rafiq and M. Abbas, Mathematical analysis to control the spread of Ebola virus epidemic through voluntary vaccination, *Eur. Phys. J. Plus* **135** (2020) 1–34.
9. N. Yazdani and A. Abbas, Pakistan adopts defensive strategies against Ebola contagion, *Arch. Pharma. Pract.* **6**(1) (2015) 13.
10. G. C. E. Mbah, I. S. Onah, Q. O. Ahman, O. C. Collins, C. C. Asogwa and C. Okoye, Mathematical modelling approach of the study of Ebola virus disease transmission dynamics in a developing country, *Afr. J. Infect. Dis.* **17**(1) (2022) 10–26.
11. A. Brettin, R. Goldthorpe, K. Weishaar and I. V. Erovenko, Ebola could be eradicated through voluntary vaccination, *Open Sci.* **5** (2018) 171591.
12. B. Yabhoub, M. Gautam, R. Shuai, Z. V. D. Driessche and P. R. Ivanek, Reproduction numbers for infections with free-living pathogens growing in the environment, *J. Biol. Dyn.* **6**(2) (2012) 923–940.
13. G. Chowell, A. Tariq and M. Kiskowski, Vaccination strategies to control Ebola epidemics in the context of variable household inaccessibility levels, *PLoS Negl.* **13**(11) (2019) 0007814.
14. J. A. Lewnard, M. L. N. Mbah, J. A. Murillo, F. L. Altice, L. Bawo, T. G. Nyenswah and A. P. Galvani, Dynamics and control of Ebola virus transmission in Montserrado, Liberia: A mathematical modelling analysis, *Lancet Infect. Dis.* **14**(12) (2014) 1189–1195.
15. A. Rachab and D. F. M. Torres, Mathematical modelling, simulation and optimal control of the 2014 Ebola outbreak in West Africa, *Discrete Dyn. Nat. Soc.* **2015**(1) (2015) 842792.
16. P. Nouvellet, T. Garske, H. L. Mills, G. N. Gilani, W. Hinsley, I. M. Blake and N. M. Ferguson, The role of rapid diagnostics in managing Ebola epidemics, *Nature* **528**(7580) (2015) 109–116.
17. F. Rao, P. S. Mandal and Y. Kang, Complicated endemics of an SIRS model with a generalized incidence under preventive vaccination and treatment controls, *Appl. Math. Model.* **67** (2019) 38–61.
18. H. Khan, M. Aslam, A. H. Rajpar, Y. M. Chu, S. Etemad, S. Rezapour and H. Ahmad, A new fractal-fractional hybrid model for studying climate change on coastal ecosystems from the mathematical point of view, *Fractals* **32**(2) (2024) 2440015.
19. A. Atangana and D. Baleanu, New fractional derivatives with non-local and non-singular kernel: Theory and application to heat transfer model, *Therm. Sci.* **20**(2) (2016) 763–769.
20. N. Khan, A. Ali, A. Ullah and Z. A. Khan, Mathematical analysis of neurological disorder under fractional order derivative, *AIMS Math.* **8**(8) (2023) 18846–18865.
21. H. Khan, S. Ahmed, J. Alzabut, A. T. Azar and J. F. Gómez-Aguilar, Nonlinear variable order system of multi-point boundary conditions with adaptive finite-time fractional-order sliding mode control, *Int. J. Dyn. Control* **12** (2024) 1–17.
22. P. A. Naik, M. Yavuz, S. Qureshi, J. Zu and S. Townley, Modeling and analysis of COVID-19 epidemics with treatment in fractional derivatives using real data from Pakistan, *Eur. Phys. J. Plus* **135**(10) (2020) 1–42.
23. M. Yavuz and N. Sene, Stability analysis and numerical computation of the fractional predator–prey model with the harvesting rate, *Fractal Fract.* **4**(3) (2020) 35.
24. F. A. Rihan, Q. M. Al-Mdallal, H. J. AlSakaji and A. Hashish, A fractional-order epidemic model with time-delay and nonlinear incidence rate, *Chaos Solitons Fract.* **126** (2019) 97–105.
25. H. G. Sun, M. M. Meerschaert, Y. Zhang, J. Zhu and W. Chen, A fractal Richards equation to capture the non-Boltzmann scaling of water transport in unsaturated media, *Adv. Water Resour.* **52** (2013) 292–295.
26. B. Ghanbari and A. Atangana, A new application of fractional Atangana–Baleanu derivatives: Designing ABC-fractional masks in image processing, *Physica A* **542** (2020) 123516.

27. A. Atangana and S. Qureshi, Modelling attractors of chaotic dynamical systems with fractal-fractional operators, *Chaos Solitons Fractals* **123** (2019) 320–337.
28. B. Xiao, Q. Huang, H. Chen, X. Chen and G. Long, A fractal model for capillary flow through a single tortuous capillary with roughened surfaces in fibrous porous media, *Fractals* **29**(1) (2021) 2150017.
29. B. Tu, B. Xiao, Y. Zhang and G. Long, An analytical model for permeability of fractal tree-like branched networks composed of converging–diverging capillaries, *Phys. Fluids* **36**(4) (2024) 043621.
30. S. Li, J. Gao, B. Xiao, Y. Zhang, G. Long and Y. Li, Fractal analysis of dimensionless permeability and Kozeny–Carman constant of spherical granular porous media with randomly distributed tree-like branching networks, *Phys. Fluids* **36**(6) (2024) 063614.
31. B. Xiao, H. Zhu, F. Chen, G. Long and Y. Li, A fractal analytical model for Kozeny-Carman constant and permeability of roughened porous media composed of particles and converging-diverging capillaries, *Powder Technol.* **420** (2023) 118256.
32. M. Liang, Y. Liu, B. Xiao, S. Yang, Z. Wang and H. Han, An analytical model for the transverse permeability of gas diffusion layer with electrical double layer effects in proton exchange membrane fuel cells, *Int. J. Hydrog. Energy* **43**(37) (2018) 17880–17888.
33. G. Long, Y. Liu, W. Xu, P. Zhou, J. Zhou, G. Xu and B. Xiao, Analysis of crack problems in multilayered elastic medium by a consecutive stiffness method, *Mathematics* **10**(23) (2022) 4403.
34. B. Q. Xiao, G. Jiang and L. Chen, A fractal study for nucleate pool boiling heat transfer of nanofluids, *Sci. China Phys. Mech. Astron.* **53** (2010) 30–37.
35. B. Q. Xiao, Prediction of heat transfer of nanofluid on critical heat flux based on fractal geometry, *Chin. Phys. B* **22**(1) (2013) 014402.
36. B. Q. Xiao, J. Fan, G. P. Jiang and L. X. Chen, Analysis of convection heat transfer mechanism in nanofluids, *Acta Phys. Sin.* **61**(15) (2012) 154401.
37. B. Q. Xiao, Y. Yang and X. F. Xu, Subcooled pool boiling heat transfer in fractal nanofluids: A novel analytical model, *Chin. Phys. B* **23**(2) (2014) 026601.
38. P. Wang, J. Gao, B. Q. Xiao, G. Long, Q. Zheng and D. Shou, The fastest capillary flow in root-like networks under gravity, *Langmuir* **40**(18) (2024) 9741–9750.
39. P. Macansantos and J. Tullao, Analysis and control of an SEIQR epidemic model with application to Ebola disease vaccination, *Vac. Res.* **8**(1) (2021) 23–35.
40. V. D. Driessche and P. J. Watmough, Reproduction numbers and sub-threshold endemic equilibria for compartmental models of disease transmission, *Math. Biosci.* **180** (2002) 29–48.
41. H. Khan, A. H. Rajpar, J. Alzabut, M. Aslam, S. Etemad and S. Rezapour, On a fractal–fractional-based modeling for influenza and its analytical results, *Qual. Theory Dyn. Syst.* **23**(2) (2024) 70.